Vandermonde Factorization of Hankel Matrix for Complex Exponential Signal Recovery— Application in Fast NMR Spectroscopy

Jiaxi Ying , Jian-Feng Cai, Di Guo, Gongguo Tang, Member, IEEE, Zhong Chen, and Xiaobo Qu

Abstract—Many signals are modeled as a superposition of exponential functions in spectroscopy of chemistry, biology, and medical imaging. This paper studies the problem of recovering exponential signals from a random subset of samples. We exploit the Vandermonde structure of the Hankel matrix formed by the exponential signal and formulate signal recovery as Hankel matrix completion with Vandermonde factorization (HVaF). A numerical algorithm is developed to solve the proposed model and its sequence convergence is analyzed theoretically. Experiments on synthetic data demonstrate that HVaF succeeds over a wider regime than the state-of-the-art nuclear-norm-minimization-based Hankel matrix completion method, while it has a less restriction on frequency separation than the state-of-the-art atomic norm minimization and fast iterative hard thresholding methods. The effectiveness of HVaF is further validated on biological magnetic resonance spectroscopy data.

Index Terms—Exponential signal, low rank, Hankel matrix completion, spectrally sparse signal, Vandermonde factorization.

I. INTRODUCTION

S IGNALS in many practical applications can be exactly or approximately modeled as a superposition of a few complex exponential functions. Examples include analog-to-digital

Manuscript received February 6, 2018; revised July 14, 2018 and August 21, 2018; accepted August 27, 2018. Date of publication September 10, 2018; date of current version September 24, 2018. The associate editor coordinating the review of this manuscript and approving it for publication was Prof. Yuantao Gu. This work was supported in part by the National Natural Science Foundation of China Under Grants 61571380, 61811530021, 61871341, U1632274, 61672335, and 61601276; in part by the Natural Science Foundation of Fujian Province of China under Grants 2018J06018 and 2016J05205; in part by the Fundamental Research Funds for the Central Universities under Grant 20720150109, in part by the Science and Technology Program of Xiamen under Grant 3502Z20183053; and in part by the Hong Kong Research Grant Council under Grant 16300616. (Corresponding author: Xiaobo Qu.)

- J. Ying, Z. Chen, and X. Qu are with the Department of Electronic Science, Fujian Provincial Key Laboratory of Plasma and Magnetic Resonance, Xiamen University, Xiamen 361005, China (e-mail: jx.ying@connect.ust.hk; chenz@xmu.edu.cn; quxiaobo@xmu.edu.cn).
- J.-F. Cai is with the Department of Mathematics, Hong Kong University of Science and Technology, Clear Water Bay, Hong Kong SAR (e-mail: jfcai@ust. hk).
- D. Guo is with the School of Computer and Information Engineering, Xiamen University of Technology, Xiamen 361024, China (e-mail: guodi@xmut.edu.cn)
- G. Tang is with the Department of Electrical Engineering and Computer Science, Colorado School of Mines, Golden, CO 80401 USA (e-mail: gtang@mines.edu).

Color versions of one or more of the figures in this paper are available online at http://ieeexplore.ieee.org.

Digital Object Identifier 10.1109/TSP.2018.2869122

conversion in electronic systems [1], antenna signals in telecommunication [2], [3], images in fluorescence microscopy [4], echo signals in medical imaging [5] and time domain signals in nuclear magnetic resonance (NMR) spectroscopy [6]–[11]. The signal of interest in these applications is a superposition of a few complex sinusoids with or without damping factors:

$$y(t) = \sum_{r=1}^{R} c_r e^{(2\pi i f_r - \tau_r)t},$$
(1)

where $f_r \in [0,1)$ is the normalized frequency, $c_r \in \mathbb{C}$ is the associated complex amplitude, R is the number of exponentials and $\tau_r \in \mathbb{R}_+$ is the damping factor. Particularly, when there is no damping factor, i.e., $\tau_r = 0$ for $r = 1, \ldots, R, y(t)$ is a spectrally sparse signal which arises from, e.g., analog-to-digital conversion [1]; otherwise, y(t) is a sum of damped complex sinusoids that characters the time domain signal, e.g., the acquired signal in biological NMR spectroscopy [6].

Throughout the paper, it is assumed that the frequencies f_r , $r=1,\ldots,R$, are distinct and normalized with respect to Nyquist frequency, thus measurements are sampled at integer values. Let $\mathbf{y} \in \mathbb{C}^{2N-1}$ be the underlying uniformly-sampled true signal $\mathbf{y} = [y(1) \ldots y(2N-1)]^T$.

In some circumstances, the measurements of the signal y are incomplete due to high experimental cost, hardware limitation, or other inevitable reasons. For example, to accelerate data acquisition, non-uniform sampling is popular in NMR spectroscopy [6]. In this paper, we aim to recover y from partial measurements $\{y_j, j \in \Omega\}$, where $\Omega \subset \{1, \dots, 2N-1\}$ with $|\Omega| = M$ (M < 2N-1) is the set of indices of the observed entries. Since the number of degrees of freedom to determine y is much smaller than the ambient dimension 2N-1 if $R \ll 2N-1$, it is possible to recover y from a small number of measurements by exploiting its inherent structure.

One line of work tries to exploit sparsity of y in the frequency domain. Spectrally sparse signals, i.e., sums of complex sinusoids without damping factors, enjoy sparse representations in the discrete Fourier transform domain if frequencies are aligned well with the discrete frequencies. In that case, the signal can be recovered from a minimal number of samples by using conventional compressed sensing [12]. However, true frequencies often take values in the continuous domain, and the resultant basis mismatch between the true frequencies and the discretized grid [13] leads to loss of sparsity and hence degrades

the performance of compressed sensing. Therefore, total variation or atomic norm [14] minimization methods were proposed to address this problem by exploiting the sparsity of \boldsymbol{y} with continuous-valued frequencies [15], [16]. Exact recovery with high probability is established for random sampling of very few measurements, provided that the frequencies $f_r, 1, \ldots, R$, enjoy good separations [15]. Several subsequent papers on this topic include [17]–[21]. Yet, currently it is still unknown how to extend atomic norm minimization to recover damped exponential signals.

Recently, the low rank structure of the Hankel matrix formed by y is exploited to recover the signal [6], [22]–[31], and the reconstruction problem can be formulated under the framework of Low Rank Hankel Matrix Completion (LRHMC),

$$\min_{\boldsymbol{x}} \operatorname{rank}(H(\boldsymbol{x})), \text{ s.t. } \mathcal{P}_{\Omega}(\boldsymbol{x}) = \mathcal{P}_{\Omega}(\boldsymbol{y}), \tag{2}$$

where H(x) denotes a Hankel matrix arranged from x; \mathcal{P}_{Ω} is the orthogonal projector onto the indices in Ω so that the j-th element of $\mathcal{P}_{\Omega}(y)$ is equal to y_j if $j \in \Omega$ and zero otherwise.

There are several existing algorithms in the literature to solve LRHMC problem (2). In particular, nuclear norm minimization is utilized as a convex relaxation for LRHMC and theoretical recovery guarantees are established [25], [26]. This approach was independently developed to recover time domain signals in biological NMR spectroscopy [6], showing great potentials to highly accelerate data acquisition with non-uniform sampling. To design more efficient algorithms, some non-convex algorithms for low-rank Hankel matrix completion were proposed in [30], [31]. However, some critical issues remain to be solved, e.g., the recovery is sensitive to frequency separation [30], [31] and the number of measurements are expected to be further reduced in fast sampling [6], [25], [26]. In addition, low rank Hankel matrix formulation has been extended to reconstruct higher-dimensional NMR spectroscopy with block Hankel matrix [9], [10] and tensors [7]. Applications of low rank Hankel matrix can also be found in magnetic resonance imaging [32]-[35].

Note that the signal of interest in this paper is a special signal function discussed in the theory of finite rate of innovation (FRI) [36]. The class of FRI signals includes a stream of (differentiated) Diracs, non-uniform splines and piecewise smooth polynomials. The conditions for perfect reconstruction from low pass filtered observation were established under ideal low-pass filters and gaussian kernels [36], or kernels satisfying Strange-Fix conditions [37]. The reconstruction scheme estimates an annihilating filter that annihilates the Fourier series coefficients of an FRI signal at consecutive low frequencies. More recently, a unified view for sampling and reconstruction in the frequency domain was proposed [38] to deal with arbitrary sampling kernels. Some robust methods were also developed to handle the noisy situations [38]–[40]. However, these methods are not originally designed for missing data recovery and thus some modifications are necessary in this situation.

In this work, we exploit the Vandermonde structure of Hankel matrix to recover complex exponential signals. A new numerical algorithm is developed to implement this approach and its convergence properties are further analysed. The extensive simulations demonstrate that, compared with state-of-the-art methods, the new approach requires fewer measurements to recover signals. Moreover, signal parameters can be accurately estimated through HVaF reconstruction even with a small frequency separation. The advantages of the proposed approach are further validated on biological NMR spectroscopy data. A preliminary account of this study was presented in a recent conference paper [41].

It is worth noting that this paper focuses on signal reconstruction rather than parameter estimation which actually is a harmonic retrieval problem. To better clarify the contributions of this work, the main differences between this work and the work [7] are summarized here. First, the signal processing problem to be solved and their applications are different. This work is to improve the fundamental 1-dimensional complex exponential signal reconstruction and is highly motivated by fast sampling in 2-dimensional NMR spectroscopy [6] while [7] was used in Ndimensional $(N \ge 3)$ spectroscopy. In addition, the new method may be extended to other applications such as magnetic resonance imaging and hyperspectral imaging, where signals in one dimension can be modelled as sum of exponentials. Second, reconstruction models are different. This work first explores Vandermonde structure of Hankel matrix in 1-dimensional exponential signal reconstruction, while the work [7] exploits the natural tensor structures of the N-dimensional exponential signal. Third, this work makes new and important contributions to signal processing. The new method achieves higher empirical phase transition and enjoys a less restriction on frequency separation, compared with the state-of-the-art spectrally sparse signal reconstruction methods [6], [15], [25], [30].

The rest of this paper is organized as follows. Section II introduces notations. In Section III, we propose the recovery method and a numerical algorithm to implement it. Section IV presents the numerical results on both synthetic and biological NMR spectroscopy data. Section V extends discussions on the proposed method and Section VI finally concludes this work and discusses future directions.

II. NOTATIONS

We first introduce the notation used throughout this paper. We denote vectors by bold lowercase letters and matrices by bold uppercase letters. The individual entries of vectors and matrices are denoted by normal font. More explicitly, the j-th entry of a vector \boldsymbol{x} is denoted by x_j ; the (i,j)-th entry of a matrix \boldsymbol{X} is denoted by \boldsymbol{X}_{ij} . The i-th row and j-th column of a matrix \boldsymbol{X} are denoted by $\boldsymbol{X}_{(i,:)}$ and $\boldsymbol{X}_{(:,j)}$, respectively. For any matrix \boldsymbol{X} , $\|\boldsymbol{X}\|_*$ and $\|\boldsymbol{X}\|_F$ denote nuclear norm and Frobenius norm, respectively. The transpose of vectors and matrices are denoted by \boldsymbol{x}^T and \boldsymbol{X}^T , while their conjugate transpose is denoted by \boldsymbol{x}^H and \boldsymbol{X}^H . The Hadamard product (also known as entrywise product) of two matrices \boldsymbol{A} and \boldsymbol{B} is $[\boldsymbol{A} \odot \boldsymbol{B}]_{ij} = A_{ij}B_{ij}$.

Operators are denoted by calligraphic letters. Let \mathcal{R} be a Hankel operator which maps a vector $\mathbf{x} \in \mathbb{C}^n$ to a Hankel matrix

 $\mathcal{R}\boldsymbol{x} \in \mathbb{C}^{n_1 \times n_2}$ with $n_1 + n_2 = n + 1$ as follows

$$\mathcal{R}: \boldsymbol{x} \in \mathbb{C}^{n_1 + n_2 - 1} \mapsto \mathcal{R} \boldsymbol{x} \in \mathbb{C}^{n_1 \times n_2}, [\mathcal{R} \boldsymbol{x}]_{ij} = x_{i+j-1},$$
 (3)

and the adjoint operator \mathcal{R}^* of \mathcal{R} is given by

$$\mathcal{R}^* : \boldsymbol{X} \in \mathbb{C}^{n_1 \times n_2} \mapsto \mathcal{R}^* \boldsymbol{X} \in \mathbb{C}^{n_1 + n_2 - 1},$$
$$[\mathcal{R}^* \boldsymbol{X}]_k = \sum_{i+j-1=k} X_{ij},$$
(4)

for any $i \in \{1, ..., n_1\}$ and $j \in \{1, ..., n_2\}$. In particular, we denote the Hankel operator by \mathcal{H} instead of \mathcal{R} when $n_1 = n_2$, i.e., constructing a square matrix.

We denote $\mathcal{G}=\mathcal{R}^*\mathcal{R}$. Obviously, \mathcal{G} is a diagonal operator satisfying $\mathcal{G}\boldsymbol{x}=\boldsymbol{W}\boldsymbol{x},\,\boldsymbol{x}\in\mathbb{C}^{n_1+n_2-1}$, where \boldsymbol{W} is a diagonal matrix and its element on the main diagonal is the number of times that an entry of vector \boldsymbol{x} is presented in the Hankel matrix. The Moore-Penrose pseudoinverse of \mathcal{R} is denoted by $\mathcal{R}^\dagger=\mathcal{G}^{-1}\mathcal{R}^*$ which satisfies $\mathcal{R}^\dagger\mathcal{R}=\mathcal{I}$, where \mathcal{I} is the identity operator.

We also define another linear operator Q_r which aims to extract the r-th column from X. For a matrix $X \in \mathbb{C}^{s_1 \times s_2}$, specifically, we define Q_r by

$$Q_r: \mathbf{X} \in \mathbb{C}^{s_1 \times s_2} \mapsto Q_r \mathbf{X} = \mathbf{X}_{(:,r)} \in \mathbb{C}^{s_1 \times 1},$$
 (5)

for any $r \in \{1, ..., s_2\}$.

Then the adjoint Q_r^* of Q_r is given by

$$Q_r^* : \boldsymbol{x} \in \mathbb{C}^{s_1 \times 1} \mapsto Q_r^* \boldsymbol{x} \in \mathbb{C}^{s_1 \times s_2},$$
$$[Q_r^* \boldsymbol{x}]_{(:,k)} = \begin{cases} \boldsymbol{x} & k = r, \\ \boldsymbol{0} & k \neq r. \end{cases} \quad \forall r \in \{1, \dots, s_2\}. \tag{6}$$

where $[\cdot]_{(:,k)}$ denotes the k-th column of a matrix, $k=1,\ldots,s_2$. Thus we have

$$[\mathcal{Q}_r^* \mathcal{Q}_r \mathbf{X}]_{(:,k)} = \begin{cases} \mathbf{X}_{(:,r)} & k = r, \\ \mathbf{0} & k \neq r. \end{cases}$$
(7)

III. THE PROPOSED METHOD

In this section, we first propose a new approach for exponential signal recovery. The proposed approach formulates the reconstruction problem as Hankel matrix completion with Vandermonde factorization. Then we develop a numerical algorithm to implement the new approach. Finally we analyse the convergence properties of the algorithm.

A. Hankel Matrix Completion With Vandermonde Factorization

Define $z_r = e^{(2\pi i f_r - \tau_r)}$ for $r = 1, \ldots, R$. It is observed that the Hankel matrix $\mathcal{H} \boldsymbol{y} \in \mathbb{C}^{N \times N}$ formed by the signal of interest

 $y \in \mathbb{C}^{2N-1}$ in (1) admits Vandermonde factorization

$$\mathcal{H}\boldsymbol{y} = \begin{bmatrix} 1 & \cdots & 1 \\ z_1 & \cdots & z_R \\ \vdots & \vdots & \vdots \\ z_1^{N-1} & \cdots & z_R^{N-1} \end{bmatrix} \begin{bmatrix} c_1 \\ \ddots \\ c_R \end{bmatrix}$$
$$\begin{bmatrix} 1 & z_1 & \cdots & z_1^{N-1} \\ \vdots & \vdots & \cdots & \vdots \\ 1 & z_R & \cdots & z_R^{N-1} \end{bmatrix} = \boldsymbol{E}\boldsymbol{\Sigma}\boldsymbol{E}^T, \tag{8}$$

where E is a Vandermone matrix and Σ is a diagonal matrix. We rewrite (8) as a form of the product of two factor matrices

$$\mathcal{H}\boldsymbol{y} = \boldsymbol{E}_L \boldsymbol{E}_R^T, \tag{9}$$

where $E_L = E\Sigma_L$ and $E_R = E\Sigma_R$ with $\Sigma_L\Sigma_R^T = \Sigma$, and Σ_L and $\Sigma_R \in \mathbb{C}^{R \times R}$ are both diagonal matrices. Clearly, (9) can be easily converted to (8) by normalizing E_L and E_R . Therefore, for ease of presentation in this paper, we also call (9) as Vandermonde factorization and E_L and E_R are with Vandermonde structure in this paper. In addition, structured matrix factorization was also explored in applications such as blind separations [42] and power spectra separations [43].

In this paper, we reconstruct complex exponential signal by imposing Vandermonde factorization on Hankel matrix:

Find
$$x, U, V$$
 (10)

subject to U and V are of Vandermonde structure,

$$\mathcal{H}oldsymbol{x} = oldsymbol{U}oldsymbol{V}^T, \quad \mathcal{P}_{\Omega}(oldsymbol{x}) = \mathcal{P}_{\Omega}(oldsymbol{y}).$$

Specifically, (10) aims to find x, which is consistent with y in Ω and the Hankel matrix formed by which can be factorized into two matrices with Vandermonde structure. From (8), it is observed that Vandermonde factorization is a special form of low rank matrix factorization; the product of factor matrices from Vandermonde factorization compose a low rank matrix, meanwhile they comply with Vandermonde structure. Therefore, (10) imposes more constraints in recovery than LRHMC in (2) and thus has a potential to achieve a better reconstruction.

Unfortunately, it is hard to directly impose Vandermonde structure on U and V, since the set of all Vandermonde matrices is non-convex and highly nonlinear, which may cause the optimization problem to be computationally intractable. In this paper, Vandermonde structure is expected by seeking each column of the matrix to be an exponential function.

Note that $\operatorname{rank}(\mathcal{R}\boldsymbol{a})=1$ if \boldsymbol{a} is a column of a matrix with Vandermonde structure. Let $\boldsymbol{A}=[\boldsymbol{a}_1,\ldots,\boldsymbol{a}_R]\in\mathbb{C}^{N\times R}$ be a matrix without zero columns. It is obvious that $R\leq\sum_{r=1}^R\operatorname{rank}(\mathcal{R}\boldsymbol{a}_r)$. More importantly, $R=\sum_{r=1}^R\operatorname{rank}(\mathcal{R}\boldsymbol{a}_r)$ if and only if \boldsymbol{A} is Vandermonde. Therefore, minimizing $\sum_{r=1}^R\operatorname{rank}(\mathcal{R}\boldsymbol{a}_r)$ will favor \boldsymbol{A} to be of Vandermonde

structure. Based on this observation, we propose

$$\min_{\boldsymbol{U}, \boldsymbol{V}, \boldsymbol{x}} \quad \sum_{r=1}^{\hat{R}} \left(\operatorname{rank}(\mathcal{R}\boldsymbol{U}_{(:,r)}) + \operatorname{rank}(\mathcal{R}\boldsymbol{V}_{(:,r)}) \right),$$
s.t. $\mathcal{H}\boldsymbol{x} = \boldsymbol{U}\boldsymbol{V}^T, \mathcal{P}_{\Omega}(\boldsymbol{x}) = \mathcal{P}_{\Omega}(\boldsymbol{y}).$ (11)

The objective function is to encourage U and V are with Vandermonde structure. However, due to the rank function involved, it is hard to solve the above minimization. Here we relax rank function by nuclear norm, and solve

$$\min_{\boldsymbol{U}, \boldsymbol{V}, \boldsymbol{x}} \quad \sum_{r=1}^{\hat{R}} (\|\mathcal{R}\boldsymbol{U}_{(:,r)}\|_* + \|\mathcal{R}\boldsymbol{V}_{(:,r)}\|_*),$$
s.t. $\mathcal{H}\boldsymbol{x} = \boldsymbol{U}\boldsymbol{V}^T, \mathcal{P}_{\Omega}(\boldsymbol{x}) = \mathcal{P}_{\Omega}(\boldsymbol{y}).$ (12)

Here both \mathcal{R} and \mathcal{H} are defined to map a vector to a Hankel matrix. By the operator \mathcal{H} , the 1-D exponential signal recovery problem is reformulated as Hankel matrix completion which has been explored in [6], [25], [27], [29], [30]. To further impose the Vandermonde structure which is first explored in our paper, we map each column of U and V to Hankel matrix by using operator \mathcal{R} and then minimize the nuclear norm of each Hankel matrix. Therefore, using two different notations helps present our contributions more clearly.

We adopt the type of $\mathcal{H}x = UV^T$ rather than symmetrical decomposition form, which is shown in (8), with using U only due to the fact that the Hankel matrix may not be exactly square when the dimension of x is even. Therefore, our proposed approach is not limited to odd dimensional signals. In addition, using the former type can find the closed form solutions of U and V directly but not for the latter.

A numerical algorithm is developed in the next subsection and the effectiveness is verified by experiments on synthetic data and realistic biological magnetic resonance spectroscopy data in Section IV.

Note that the exact number of exponentials R is usually unknown in practice especially in the case of non-uniform sampling, hence our algorithm needs to preset the number of exponentials. It will be shown in Section IV that the proposed algorithm can succeed in recovering the signal with high probability even when the preset number of exponentials \hat{R} is greatly larger than R.

B. Numerical Algorithm

In this subsection, we develop a numerical algorithm to implement the proposed method. Recall that Q_r defined in (5). We rewrite (12) as its equivalence

$$\min_{\boldsymbol{U}, \boldsymbol{V}, \boldsymbol{x}} \quad \sum_{r=1}^{R} (\|\mathcal{R}\mathcal{Q}_{r}\boldsymbol{U}\|_{*} + \|\mathcal{R}\mathcal{Q}_{r}\boldsymbol{V}\|_{*}),$$
s.t. $\mathcal{H}\boldsymbol{x} = \boldsymbol{U}\boldsymbol{V}^{T}, \mathcal{P}_{\Omega}(\boldsymbol{x}) = \mathcal{P}_{\Omega}(\boldsymbol{y}).$ (13)

To solve (13), we develop an algorithm based on half quadratic methods with continuation [44], [45] for its advantage in handling multi-variable optimization [46]. We introduce

the term $\|\mathcal{H}x - UV^T\|_F^2$ to keep $\mathcal{H}x$ close enough to UV^T instead of the exact constraint $\mathcal{H}x = UV^T$. Now, we have the following optimization:

$$\min_{oldsymbol{U},oldsymbol{V},oldsymbol{x}} \;\; \sum_{r=1}^{\hat{R}} \left(\left\| \mathcal{R} \mathcal{Q}_r oldsymbol{U}
ight\|_* + \left\| \mathcal{R} \mathcal{Q}_r oldsymbol{V}
ight\|_*
ight) + rac{eta}{2} \left\| \mathcal{H} oldsymbol{x} - oldsymbol{U} oldsymbol{V}^T
ight\|_F^2 \, ,$$

s.t.
$$\mathcal{P}_{\Omega}(\mathbf{x}) = \mathcal{P}_{\Omega}(\mathbf{y})$$
. (14)

When $\beta \to \infty$, the solution to (14) is approaching the one to (13). The challenge in solving (14) is that the nuclear norm terms are non-smooth and non-separable simultaneously. To decouple the non-smoothness and the non-separability, we introduce some auxiliary variables into (14) [47], and then reformulate the problem (14) as the following equivalent form:

$$\min_{\substack{\boldsymbol{U},\boldsymbol{V},\boldsymbol{x},\boldsymbol{B}_r,\boldsymbol{C}_r\\r=1,\dots,\hat{R}}}\sum_{r=1}^{\hat{R}}\left(\|\boldsymbol{B}_r\|_*+\|\boldsymbol{C}_r\|_*\right)+\frac{\beta}{2}\left\|\mathcal{H}\boldsymbol{x}-\boldsymbol{U}\boldsymbol{V}^T\right\|_F^2,$$

s.t.
$$\boldsymbol{B}_r = \mathcal{R}\mathcal{Q}_r \boldsymbol{U}, \ \boldsymbol{C}_r = \mathcal{R}\mathcal{Q}_r \boldsymbol{V}, \ r \in \{1, \dots, \hat{R}\},$$

$$\mathcal{P}_{\Omega}(\boldsymbol{x}) = \mathcal{P}_{\Omega}(\boldsymbol{y}). \tag{15}$$

In (15), the first two terms are non-smooth but separable, and the other terms are smooth, which makes it easier to develop numerical algorithms. With a fixed β , we use Alternating Direction Method of Multipliers (ADMM) to solve (15).

In the following, we first present an overview of the proposed algorithm, and then describe how to update each variable of the algorithm in detail. Let $\mathcal{B} = (B_1, \ldots, B_{\hat{R}})$, $\mathcal{C} = (C_1, \ldots, C_{\hat{R}})$, $\mathcal{D} = (D_1, \ldots, D_{\hat{R}})$ and $\mathcal{M} = (M_1, \ldots, M_{\hat{R}})$. The augmented Lagrangian function of (15) is

$$\mathcal{L}_{\mu}(\boldsymbol{U}, \boldsymbol{V}, \boldsymbol{x}, \mathcal{B}, \mathcal{D}, \mathcal{C}, \mathcal{M}) = \frac{\beta}{2} \| \mathcal{H} \boldsymbol{x} - \boldsymbol{U} \boldsymbol{V}^T \|_F^2$$
$$+ \sum_{r} \hat{\boldsymbol{\Gamma}} \left(\| \boldsymbol{B}_r \|_* + \langle \boldsymbol{D}_r, \mathcal{R} \mathcal{Q}_r \boldsymbol{U} - \boldsymbol{B}_r \rangle + \frac{\mu}{2} \| \mathcal{R} \mathcal{Q}_r \boldsymbol{U} - \boldsymbol{B}_r \|_F^2 \right)$$

$$+\sum_{r=1}^{\hat{R}} \left(\|\boldsymbol{C}_r\|_* + \langle \boldsymbol{M}_r, \mathcal{R} \mathcal{Q}_r \boldsymbol{V} - \boldsymbol{C}_r \rangle + \frac{\mu}{2} \|\mathcal{R} \mathcal{Q}_r \boldsymbol{V} - \boldsymbol{C}_r\|_F^2 \right).$$
(16)

where D_r and M_r are the Lagrange multipliers, $r=1,\cdots,\bar{R}$. We present an ADMM iterative scheme to successively minimize $\mathcal{L}_{\mu}(U,V,x,\mathcal{B},\mathcal{C},\mathcal{D},\mathcal{M})$ as follows:

$$\min_{\boldsymbol{U}} \mathcal{L}_{\mu^k}(\boldsymbol{U}, \boldsymbol{V}^k, \boldsymbol{x}^k, \mathcal{B}^k, \mathcal{C}^k, \mathcal{D}^k, \mathcal{M}^k)$$
 (17)

$$\min_{\boldsymbol{V}} \mathcal{L}_{\mu^k}(\boldsymbol{U}^{k+1}, \boldsymbol{V}, \boldsymbol{x}^k, \mathcal{B}^k, \mathcal{C}^k, \mathcal{D}^k, \mathcal{M}^k)$$
 (18)

$$\min_{\boldsymbol{x}} \mathcal{L}_{\mu^k}(\boldsymbol{U}^{k+1}, \boldsymbol{V}^{k+1}, \boldsymbol{x}, \mathcal{B}^k, \mathcal{C}^k, \mathcal{D}^k, \mathcal{M}^k)$$
 (19)

s.t.
$$\mathcal{P}_{\Omega}(\boldsymbol{x}) = \mathcal{P}_{\Omega}(\boldsymbol{y})$$
.

$$\min_{\mathcal{B}} \mathcal{L}_{\mu^k}(\boldsymbol{U}^{k+1}, \boldsymbol{V}^{k+1}, \boldsymbol{x}^{k+1}, \mathcal{B}, \mathcal{C}^k, \mathcal{D}^k, \mathcal{M}^k)$$
 (20)

$$\min_{\mathcal{C}} \mathcal{L}_{\mu^k}(\boldsymbol{U}^{k+1}, \boldsymbol{V}^{k+1}, \boldsymbol{x}^{k+1}, \mathcal{B}^{k+1}, \mathcal{C}, \mathcal{D}^k, \mathcal{M}^k)$$
 (21)

$$D_r^{k+1} = D_r^k + \mu^k (\mathcal{R} \mathcal{Q}_r U^{k+1} - B_r^{k+1})$$

$$\forall r \in \{1, \dots, \hat{R}\}.$$

$$M_r^{k+1} = M_r^k + \mu^k (\mathcal{R} \mathcal{Q}_r V^{k+1} - C_r^{k+1})$$

$$\forall r \in \{1, \dots, \hat{R}\}.$$
(22)

1) Update \boldsymbol{U} and \boldsymbol{V}

To update the variable U, the optimization problem (17) is written as follows:

$$\min_{\boldsymbol{U}} \frac{\beta}{2} \left\| \mathcal{H} \boldsymbol{x}^{k} - \boldsymbol{U} \left(\boldsymbol{V}^{k} \right)^{T} \right\|_{F}^{2} + \frac{\mu^{k}}{2} \sum_{r=1}^{\hat{R}} \left\| \mathcal{R} \mathcal{Q}_{r} \boldsymbol{U} - \boldsymbol{B}_{r}^{k} + (\mu^{k})^{-1} \boldsymbol{D}_{r}^{k} \right\|_{F}^{2}. \tag{24}$$

Since (24) is a least square problem, its solution is obtained by solving a system of linear equations as follows

$$\mu^{k} \sum_{r=1}^{R} \mathcal{Q}_{r}^{*} \mathcal{R}^{*} \mathcal{R} \mathcal{Q}_{r} \boldsymbol{U} + \beta \boldsymbol{U} (\boldsymbol{V}^{k})^{T} \operatorname{conj}(\boldsymbol{V}^{k})$$

$$= \sum_{r=1}^{\hat{R}} \mu^{k} \mathcal{Q}_{r}^{*} \mathcal{R}^{*} \left(\boldsymbol{B}_{r}^{k} - \boldsymbol{D}_{r}^{k} / \mu^{k} \right) + \beta \left(\mathcal{H} \boldsymbol{x}^{k} \right) \operatorname{conj}(\boldsymbol{V}^{k}),$$
(25)

where $conj(\cdot)$ denotes the conjugate of a matrix.

Similar to the case of U, we can update V by solving the following equation

$$\min_{\mathbf{V}} \frac{\beta}{2} \| \mathcal{H} \mathbf{x}^k - \mathbf{U}^{k+1} \mathbf{V}^T \|_F^2
+ \frac{\mu^k}{2} \sum_{r=1}^{\hat{R}} \| \mathcal{R} \mathcal{Q}_r \mathbf{V} - \mathbf{C}_r^k + (\mu^k)^{-1} \mathbf{M}_r^k \|_F^2,$$
(26)

and its solution can be obtained by

$$\mu^{k} \sum_{r=1}^{\hat{R}} \mathcal{Q}_{r}^{*} \mathcal{R}^{*} \mathcal{R} \mathcal{Q}_{r} \boldsymbol{V} + \beta \boldsymbol{V} (\boldsymbol{U}^{k+1})^{T} \operatorname{conj}(\boldsymbol{U}^{k+1})$$

$$= \sum_{r=1}^{\hat{R}} \mu^{k} \mathcal{Q}_{r}^{*} \mathcal{R}^{*} \left(\boldsymbol{C}_{r}^{k} - \boldsymbol{M}_{r}^{k} / \mu^{k} \right) + \beta \left(\mathcal{H} \boldsymbol{x}^{k} \right)^{T} \operatorname{conj}(\boldsymbol{U}^{k+1}).$$
(27)

The specific closed-form solution of U and V are given in Appendix.

2) Update x

We update the variable x by solving

$$\min_{\boldsymbol{x}} \left\| \mathcal{H} \boldsymbol{x} - \boldsymbol{U}^{k+1} (\boldsymbol{V}^{k+1})^T \right\|_{F}^{2}, \text{ s.t. } \mathcal{P}_{\Omega}(\boldsymbol{x}) = \mathcal{P}_{\Omega}(\boldsymbol{y}).$$
 (28)

By introducing Lagrangian multiplier d for the constraint $\mathcal{P}_{\Omega}(x) = \mathcal{P}_{\Omega}(y)$, we write the Lagrangian function of (28) as follows:

$$F(\boldsymbol{x}, \boldsymbol{d}) = \left\| \mathcal{H} \boldsymbol{x} - \boldsymbol{U}^{k+1} (\boldsymbol{V}^{k+1})^T \right\|_F^2 + \langle \boldsymbol{d}, \mathcal{P}_{\Omega}(\boldsymbol{x}) - \mathcal{P}_{\Omega}(\boldsymbol{y}) \rangle.$$
(29)

By setting $\nabla_{(x,d)}F = \mathbf{0}$, we have the Karush-Kuhn-Tucker (KKT) conditions

$$egin{aligned} \left(\mathcal{H}^*\mathcal{H}oldsymbol{x}-\mathcal{H}^*\left(oldsymbol{U}^{k+1}\left(oldsymbol{V}^{k+1}
ight)^T
ight)
ight)-\mathcal{P}_{\Omega}(oldsymbol{d}) = oldsymbol{0}. \ &\mathcal{P}_{\Omega}(oldsymbol{x})-\mathcal{P}_{\Omega}(oldsymbol{y}) = oldsymbol{0}. \end{aligned}$$

By deriving the KKT conditions simply, one has

$$\boldsymbol{x}^{k+1} = \mathcal{P}_{\Omega}(\boldsymbol{y}) + \mathcal{P}_{\Omega^{C}}\left(\boldsymbol{W}^{-1}\left(\mathcal{H}^{*}\left(\boldsymbol{U}^{k+1}\left(\boldsymbol{V}^{k+1}\right)^{T}\right)\right)\right). \tag{30}$$

where Ω^{C} is the complement of Ω , i.e., the set of indices of the unobserved entries, and W is a constant matrix as introduced in Section II.

3) Update B_r and C_r

To update B_r , we solve the following sub-problem,

$$\min_{\boldsymbol{B}_r} \|\boldsymbol{B}_r\|_* + \left\langle \boldsymbol{D}_r^k, \mathcal{R} \mathcal{Q}_r \boldsymbol{U}^{k+1} - \boldsymbol{B}_r \right\rangle + \frac{\mu^k}{2} \|\mathcal{R} \mathcal{Q}_r \boldsymbol{U}^{k+1} - \boldsymbol{B}_r\|_F^2.$$
(31)

Following [48], the closed-form solution of (31) is

$$\boldsymbol{B}_{r}^{k+1} = S_{1/\mu^{k}} \left(\mathcal{R} \mathcal{Q}_{r} \boldsymbol{U}^{k+1} + 1/\mu^{k} \boldsymbol{D}_{r}^{k} \right),$$
 (32)

where S is the soft singular value thresholding operator [48] with threshold $1/\mu^k$. Similar to update B_r , we can update C_r by

$$\min_{\boldsymbol{C}_r} \|\boldsymbol{C}_r\|_* + \langle \boldsymbol{M}_r^k, \mathcal{R} \mathcal{Q}_r \boldsymbol{V}^{k+1} - \boldsymbol{C}_r \rangle
+ \frac{\mu^k}{2} \|\mathcal{R} \mathcal{Q}_r \boldsymbol{V}^{k+1} - \boldsymbol{C}_r\|_F^2,$$
(33)

and its solution is

$$\boldsymbol{C}_r^{k+1} = S_{1/\mu^k} \left(\mathcal{R} \mathcal{Q}_r \boldsymbol{V}^{k+1} + 1/\mu^k \boldsymbol{M}_r^k \right)$$
 (34)

For a fixed nonzero β , the solution to (14) only yields an approximation to the solution to (11). To obtain a better solution, we apply a continuation scheme in which we gradually improve β to $+\infty$. This algorithm can also be accelerated by adaptively changing μ . An efficient strategy [49], [50] is to increase μ^k iteratively by $\mu^{k+1} = \rho \mu^k$, where $\rho \in (1, 1.1]$. The overall algorithm is summarized in Algorithm 1.

In real applications, the measurements are usually contaminated by Gaussian noise. To recover the signal from noisy measurements, we propose the following optimization

$$\min_{\boldsymbol{U}, \boldsymbol{V}, \boldsymbol{x}} \sum_{r=1}^{R} (\|\mathcal{R} \mathcal{Q}_{r} \boldsymbol{U}\|_{*} + \|\mathcal{R} \mathcal{Q}_{r} \boldsymbol{V}\|_{*}) + \frac{\beta}{2} \|\mathcal{H} \boldsymbol{x} - \boldsymbol{U} \boldsymbol{V}^{T}\|_{F}^{2} + \frac{\lambda}{2} \|\mathcal{P}_{\Omega}(\boldsymbol{x}) - \mathcal{P}_{\Omega}(\boldsymbol{y})\|_{2}^{2}.$$
(35)

All the variables except \boldsymbol{x} can be updated as above. We update the variable \boldsymbol{x} by

$$\min_{oldsymbol{x}} rac{eta}{2} \left\| \mathcal{H} oldsymbol{x} - oldsymbol{U}^{k+1} \left(oldsymbol{V}^{k+1}
ight)^T
ight\|_F^2 + rac{\lambda}{2} \left\| \mathcal{P}_{\Omega}(oldsymbol{x}) - \mathcal{P}_{\Omega}(oldsymbol{y})
ight\|_2^2,$$

Algorithm 1: Algorithm for Hankel Matrix Completion With Vandermonde Factorization (HVaF).

- 1: Initialization: $U, V, x = \mathcal{P}_{\Omega}(y), \beta = 2^5, \beta_{\text{max}} = 2^{30}, \mu^0 = 10^{-2}, \text{ and } \rho = 1.05.$
- 2: while $\beta \leq \beta_{\max}$ do
- 3: Update U, V by solving (25) and (27);
- 4: Update x by solving (30);
- 5: For r = 1 to \hat{R} , update B_r and C_r by solving (32) and (34):
- 6: For r = 1 to \hat{R} , update D_r and M_r by solving (22) and (23);
- 7: Update μ by $\mu^{k+1} = \rho \mu^k$;
- 8: If $\|\Delta x\| = \|x_{\text{last}} x\|/\|x_{\text{last}}\| > 10^{-7}$, $x_{\text{last}} \leftarrow x$, go to step 3; otherwise, go to step 9;
- 9: $\beta \leftarrow 2\beta$;
- 10: end while

and thus

$$\boldsymbol{x}^{k+1} = (\beta \boldsymbol{W} + \lambda \mathcal{P}_{\Omega}^* \mathcal{P}_{\Omega})^{-1}$$

$$\left(\beta \left(\mathcal{H}^* \left(\boldsymbol{U}^{k+1} \left(\boldsymbol{V}^{k+1}\right)^T\right)\right) + \lambda \mathcal{P}_{\Omega}^* \mathcal{P}_{\Omega}(\boldsymbol{y})\right). \quad (36)$$

The variable x is updated by (36) in recovering the realistic biological NMR spectroscopy data as shown in Section IV-B.

C. Convergence Analysis

In this section, we analyse the convergence of Algorithm 1. In Theorem 1, we show that the sequences $\{U^k\}$, $\{V^k\}$, $\{x^k\}$, $\{\mathcal{B}^k\}$ and $\{\mathcal{C}^k\}$ generated by Algorithm 1 with fixed β converge. Theorem 1: The sequences $\{U^k\}$, $\{V^k\}$, $\{x^k\}$, $\{\mathcal{B}^k\}$ and $\{\mathcal{C}^k\}$ generated by Algorithm 1 with fixed β are all convergent.

Before proving the convergence properties of the algorithm, we first prove the boundedness of multipliers and some variables generated by Algorithm 1.

 $\begin{array}{l} \textit{Lemma 1:} \text{ The sequences } \{\boldsymbol{D}_r^k\} \text{ and } \{\boldsymbol{M}_r^k\}, r=1,\dots,\hat{R}, \\ \text{are bounded, where } \boldsymbol{D}_r^{k+1} = \boldsymbol{D}_r^k + \mu^k(\mathcal{R}\mathcal{Q}_r\boldsymbol{U}^{k+1} - \boldsymbol{B}_r^{k+1}) \\ \text{and } \boldsymbol{M}_r^{k+1} = \boldsymbol{M}_r^k + \mu^k(\mathcal{R}\mathcal{Q}_r\boldsymbol{V}^{k+1} - \boldsymbol{C}_r^{k+1}). \end{array}$

Proof: The optimality condition of (31) gives

$$\mathbf{0} \in \partial \left\| \boldsymbol{B}_r^{k+1} \right\|_* - \boldsymbol{D}_r^k - \mu^k (\mathcal{R} \mathcal{Q}_r \boldsymbol{U}^{k+1} - \boldsymbol{B}_r^{k+1}),$$

which combined with (22) implies

$$\boldsymbol{D}_{r}^{k+1}\in\partial\left\|\boldsymbol{B}_{r}^{k+1}\right\|_{*}.$$

According to [48], each element of the subgradient of the nuclear norm is bounded by 1 in spectral norm. Therefore $\|\boldsymbol{D}_r^{k+1}\|_2 \leq 1$ and hence the sequence $\{\boldsymbol{D}_r^k\}$ is bounded for all $r \in \{1,\ldots,\hat{R}\}$. The boundedness of $\{\boldsymbol{M}_r^k\}$ can be proved similarly.

Lemma 2: The sequences $\{U^k\}$, $\{V^k\}$, $\{x^k\}$, $\{\mathcal{B}^k\}$ and $\{\mathcal{C}^k\}$ produced by Algorithm 1 with fixed β are all bounded.

Proof: The augmented Lagrangian function satisfies

$$egin{aligned} &\mathcal{L}_{\mu^k}(oldsymbol{U}^{k+1},oldsymbol{V}^{k+1},oldsymbol{x}^{k+1},\mathcal{B}^{k+1},\mathcal{C}^{k+1},\mathcal{D}^{k+1},\mathcal{M}^k) \ &\leq \mathcal{L}_{\mu^k}(oldsymbol{U}^k,oldsymbol{V}^k,oldsymbol{x}^k,\mathcal{B}^k,\mathcal{C}^k,\mathcal{D}^k,\mathcal{M}^k) \ &= \mathcal{L}_{\mu^{k-1}}(oldsymbol{U}^k,oldsymbol{V}^k,oldsymbol{x}^k,\mathcal{B}^k,\mathcal{C}^k,\mathcal{D}^k,\mathcal{M}^{k-1}) \ &+ \sum_{r=1}^{\hat{R}} \left\langle oldsymbol{M}_r^k - oldsymbol{M}_r^{k-1},\mathcal{R}\mathcal{Q}_roldsymbol{V}^k - oldsymbol{C}_r^k
ight
angle \\ &+ \frac{\mu^k - \mu^{k-1}}{2} \left\| \mathcal{R}\mathcal{Q}_roldsymbol{V}^k - oldsymbol{C}_r^k
ight\|_F^2 \ &= \mathcal{L}_{\mu^{k-1}}(oldsymbol{U}^k,oldsymbol{V}^k,oldsymbol{x}^k,\mathcal{B}^k,\mathcal{C}^k,\mathcal{D}^k,\mathcal{M}^{k-1}) \ &+ \frac{\mu^k + \mu^{k-1}}{2(\mu^{k-1})^2} \sum_{r=1}^{\hat{R}} \left\| oldsymbol{M}_r^k - oldsymbol{M}_r^{k-1}
ight\|_F^2. \end{aligned}$$

Summing it over k gives

$$\mathcal{L}_{\mu^{k}}(\boldsymbol{U}^{k+1}, \boldsymbol{V}^{k+1}, \boldsymbol{x}^{k+1}, \mathcal{B}^{k+1}, \mathcal{C}^{k+1}, \mathcal{D}^{k+1}, \mathcal{M}^{k})$$

$$\leq \mathcal{L}_{\mu^{0}}(\boldsymbol{U}^{1}, \boldsymbol{V}^{1}, \boldsymbol{x}^{1}, \mathcal{B}^{1}, \mathcal{C}^{1}, \mathcal{D}^{1}, \mathcal{M}^{0})$$

$$+ \sum_{j=1}^{k} \left(\frac{\mu^{j} + \mu^{j-1}}{2(\mu^{j-1})^{2}} \sum_{r=1}^{\hat{R}} \left\| \boldsymbol{M}_{r}^{j} - \boldsymbol{M}_{r}^{j-1} \right\|_{F}^{2} \right)$$

$$\leq \mathcal{L}_{\mu^{0}}(\boldsymbol{U}^{1}, \boldsymbol{V}^{1}, \boldsymbol{x}^{1}, \mathcal{B}^{1}, \mathcal{C}^{1}, \mathcal{D}^{1}, \mathcal{M}^{0})$$

$$+ \left(\sum_{j=1}^{k} \frac{\mu^{j} + \mu^{j-1}}{2(\mu^{j-1})^{2}} \right) \left(\max_{j=1}^{k} \sum_{r=1}^{\hat{R}} \left\| \boldsymbol{M}_{r}^{j} - \boldsymbol{M}_{r}^{j-1} \right\|_{F}^{2} \right).$$
(37)

Since $\{\boldsymbol{M}_r^k\}$ is bounded, $\max_{j=1}^{\infty}\sum_{r=1}^{\hat{R}}\left\|\boldsymbol{M}_r^j-\boldsymbol{M}_r^{j-1}\right\|_F^2$ is bounded. Furthermore, because of $\mu^{k+1}=\rho\mu^k$ and $\rho\in(1,\ 1.1],$

$$\sum_{j=1}^{\infty} \frac{\mu^j + \mu^{j-1}}{2(\mu^{j-1})^2} = \frac{\rho(\rho+1)}{2\mu^0(\rho-1)} < \infty.$$

Hence, $\{\mathcal{L}_{\mu^{k-1}}(\boldsymbol{U}^k, \boldsymbol{V}^k, \boldsymbol{x}^k, \mathcal{B}^k, \mathcal{C}^k, \mathcal{D}^k, \mathcal{M}^{k-1})\}$ is bounded. Similarly, $\{\mathcal{L}_{\mu^{k-1}}(\boldsymbol{U}^k, \boldsymbol{V}^k, \boldsymbol{x}^k, \mathcal{B}^k, \mathcal{C}^k, \mathcal{D}^{k-1}, \mathcal{M}^{k-1})\}$ is also bounded. We further have that

$$\begin{split} &\frac{\beta}{2} \left\| \mathcal{H} \boldsymbol{x}^{k} - \boldsymbol{U}^{k} \left(\boldsymbol{V}^{k} \right)^{T} \right\|_{F}^{2} + \sum_{r=1}^{\hat{R}} (\left\| \boldsymbol{B}_{r}^{k} \right\|_{*} + \left\| \boldsymbol{C}_{r}^{k} \right\|_{*}) \\ &= \mathcal{L}_{\mu^{k-1}} (\boldsymbol{U}^{k}, \boldsymbol{V}^{k}, \boldsymbol{x}^{k}, \mathcal{B}^{k}, \mathcal{C}^{k}, \mathcal{D}^{k-1}, \mathcal{M}^{k-1}) \\ &- \frac{1}{\mu^{k-1}} \sum_{r=1}^{\hat{R}} \left(\langle \boldsymbol{D}_{r}^{k-1}, \boldsymbol{D}_{r}^{k} - \boldsymbol{D}_{r}^{k-1} \rangle + \frac{1}{2} \left\| \boldsymbol{D}_{r}^{k} - \boldsymbol{D}_{r}^{k-1} \right\|_{F}^{2} \right) \\ &- \frac{1}{\mu^{k-1}} \sum_{r=1}^{\hat{R}} \left(\langle \boldsymbol{M}_{r}^{k-1}, \boldsymbol{M}_{r}^{k} - \boldsymbol{M}_{r}^{k-1} \rangle + \frac{1}{2} \left\| \boldsymbol{M}_{r}^{k} - \boldsymbol{M}_{r}^{k-1} \right\|_{F}^{2} \right). \end{split}$$

Since all terms on the right hand side are bounded, the left hand side is bounded. Thus, $\{\mathcal{B}^k\}$ and $\{\mathcal{C}^k\}$ are bounded.

Finally, we have $\mathcal{RQ}_r U^{k+1} = B_r^{k+1} + (D_r^{k+1} - D_r^k)/\mu^k$ and $\mathcal{RQ}_r V^{k+1} = C_r^{k+1} + (M_r^{k+1} - M_r^k)/\mu^k$, $r = 1, \ldots, \hat{R}$. Also, \mathcal{RQ}_r is injective. Therefore, the sequences $\{U^k\}$ and $\{V^k\}$ are also bounded. According to (30), $\{x^k\}$ is bounded, too.

Now we are ready to prove Theorem 1.

Proof of Theorem 1: The updating formula (22) and the optimality condition of (24) with respect to \mathbf{U}^{k+1} imply

$$\sum_{r=1}^{\hat{R}} \left(\mu^{k} \mathcal{Q}_{r}^{*} \mathcal{R}^{*} \mathcal{R} \mathcal{Q}_{r} U^{k+1} - \mu^{k} \mathcal{Q}_{r}^{*} \mathcal{R}^{*} \boldsymbol{B}_{r}^{k} + \mathcal{Q}_{r}^{*} \mathcal{R}^{*} \boldsymbol{D}_{r}^{k} \right)$$

$$+ \beta \boldsymbol{U}^{k+1} \left(\boldsymbol{V}^{k} \right)^{T} \operatorname{conj}(\boldsymbol{V}^{k}) - \beta (\mathcal{R} \boldsymbol{x}^{k}) \operatorname{conj}(\boldsymbol{V}^{k})$$

$$= \mu^{k} \sum_{r=1}^{\hat{R}} \mathcal{Q}_{r}^{*} \mathcal{R}^{*} \left(\mathcal{R} \mathcal{Q}_{r} (\boldsymbol{U}^{k+1} - \boldsymbol{U}^{k}) + \frac{1}{\mu^{k}} \boldsymbol{D}_{r}^{k} - \frac{1}{\mu^{k-1}} \boldsymbol{D}_{r}^{k-1} \right)$$

$$+ \mu^{k} \sum_{r=1}^{\hat{R}} \mathcal{Q}_{r}^{*} \mathcal{R}^{*} \left(\mathcal{R} \mathcal{Q}_{r} \boldsymbol{U}^{k} - \boldsymbol{B}_{r}^{k} + \frac{1}{\mu^{k-1}} \boldsymbol{D}_{r}^{k-1} \right)$$

$$+ \beta \boldsymbol{U}^{k+1} \left(\boldsymbol{V}^{k} \right)^{T} \operatorname{conj}(\boldsymbol{V}^{k}) - \beta (\mathcal{R} \boldsymbol{x}^{k}) \operatorname{conj}(\boldsymbol{V}^{k}) = \mathbf{0}.$$

Since $\sum_{r=1}^{\hat{R}} \mathcal{Q}_r^* \mathcal{R}^* \mathcal{R} \mathcal{Q}_r (\boldsymbol{U}^{k+1} - \boldsymbol{U}^k)$ can be denoted by $\boldsymbol{T} \odot (\boldsymbol{U}^{k+1} - \boldsymbol{U}^k)$, where \boldsymbol{T} is a constant matrix (the specific form of \boldsymbol{T} can be seen in the Appendix) and \odot denotes Hadamard product, we have

$$\begin{split} & \boldsymbol{T} \odot (\boldsymbol{U}^{k+1} - \boldsymbol{U}^k) \\ &= \frac{\beta}{\mu^k} \left((\mathcal{R}\boldsymbol{x}^k) \mathrm{conj}(\boldsymbol{V}^k) - \boldsymbol{U}^{k+1} \left(\boldsymbol{V}^k \right)^T \mathrm{conj}(\boldsymbol{V}^k) \right) \\ &- \frac{1}{\mu^k} \sum_{r=1}^{\hat{R}} \mathcal{Q}_r^* \mathcal{R}^* ((\rho+1) \boldsymbol{D}_r^k - \rho \boldsymbol{D}_r^{k-1}) := \frac{\boldsymbol{G}^k}{\mu^k}. \end{split}$$

By Lemma 2, the sequence $\{G_k\}$ is bounded, and denote δ its upper bound. We have $\|G_k\|_F \leq \delta$ for all k. Then, for any m and any $n \geq m$,

$$\begin{split} & \| \boldsymbol{T} \odot (\boldsymbol{U}^{n} - \boldsymbol{U}^{m}) \|_{F} \leq \left\| \boldsymbol{T} \odot (\boldsymbol{U}^{n} - \boldsymbol{U}^{n-1}) \right\|_{F} \\ & + \left\| \boldsymbol{T} \odot (\boldsymbol{U}^{n-1} - \boldsymbol{U}^{n-2}) \right\|_{F} + \ldots + \left\| \boldsymbol{T} \odot (\boldsymbol{U}^{m+1} - \boldsymbol{U}^{m}) \right\|_{F} \\ & = \frac{\left\| \boldsymbol{G}^{n-1} \right\|_{F}}{\mu^{n-1}} + \frac{\left\| \boldsymbol{G}^{n-2} \right\|_{F}}{\mu^{n-2}} + \ldots + \frac{\left\| \boldsymbol{G}^{m} \right\|_{F}}{\mu^{m}} \\ & \leq \frac{\delta}{\mu^{m}} \left(\frac{1}{\rho^{n-m-1}} + \frac{1}{\rho^{n-m-2}} + \ldots + 1 \right) \leq \frac{\delta \rho}{\mu^{m} (\rho - 1)}, \end{split}$$

Since $\frac{\delta\rho}{\mu^m(\rho-1)} \to 0$, $\{\boldsymbol{T} \odot \boldsymbol{U}^k\}$ is a Cauchy sequence. Therefore, by the fact that \boldsymbol{T} has no zero entry, $\{\boldsymbol{U}^k\}$ is a Cauchy sequence and hence convergent. Similarly, $\{\boldsymbol{V}^k\}$ is also convergent. With this, since by (30) \boldsymbol{x}^k is a continuous function of \boldsymbol{U}^k and \boldsymbol{V}^k , the sequence $\{\boldsymbol{x}^k\}$ is convergent.

It remains to show the boundedness of $\{\mathcal{B}^k\}$ and $\{\mathcal{C}^k\}$. By (22), we have $\boldsymbol{B}_r^{k+1} = \mathcal{R}\mathcal{Q}_r\boldsymbol{U}^{k+1} - (\boldsymbol{D}_r^{k+1} - \boldsymbol{D}_r^k)/\mu^k$. Furthermore, $\{\boldsymbol{U}^k\}$ is convergent, $\{\boldsymbol{D}_r^k\}$ is bounded, and $\lim_{k\to\infty}\mu^k = \infty$. Therefore, $\{\boldsymbol{B}_r^k\}$ is convergent for each

$$r \in \{1, \dots, \hat{R}\}$$
 and then $\{\mathcal{B}^k\}$ is convergent. Similarly, $\{\mathcal{C}^k\}$ is also convergent. \square

D. Computational Complexity

The main running time of the algorithm is dominated by performing singular value decomposition (SVD) for the singular value thresholding operator. Consider to recover a signal $\boldsymbol{x} \in \mathbb{C}^{2N-1}$ with the number of estimated exponentials \hat{R} . The SVD is performed on the Hankel matrix with the size of $0.5N \times 0.5N$, and thus the total time complexity of SVD in each iteration is $O(\hat{R}N^3)$.

IV. NUMERICAL EXPERIMENTS

In this section, we evaluate the performance of the proposed HVaF on synthetic data and realistic biological NMR spectroscopy data. For synthetic data, the HVaF is compared with three state-of-the-art algorithms, ANM [15], EMaC [25], FIHT [30]. ANM and EMaC are implemented using CVX [51]. For the realistic NMR data, the HVaF is compared with the state-of-the-art LRHM method [6]. All the compared methods are conducted using publicly available codes with default parameters. Here the comparisons with the method in [31] is omitted because the method in [31] together with EMaC and FIHT still belongs to the framework of LRHMC where the complex exponential signal recovery problem is formulated as low rank Hankel matrix completion.

A. Synthetic Data

We conduct a series of numerical experiments to examine the phase transition for exact recovery and estimate signal parameters. Superpositions of undamped and damped complex sinusoids are used as test signals. We follow the setup in [26], [30] to generate the test signals. Specifically, the true signal $y=[y_1,\ldots,y_{127}]^T$ where $y_k=\sum_{r=1}^R c_r e^{i2\pi f_r k}$ and $y_k=\sum_{r=1}^R c_r e^{(i2\pi f_r - \tau_r)k}, \ k=1,\ldots,127,$ for undamped and damped complex sinusoids, respectively. Each frequency f_r is drawn from the interval [0,1) uniformly at random, and each complex amplitude c_r is complex coefficients that satisfies the model $c_r = (1 + 10^{0.5m_r})e^{i2\pi\theta_r}$ with m_r and θ_r being uniformly randomly sampled from the interval [0, 1]. The damping parameters τ_r follow the model $\tau_r = 1/(10 + 30n_r)$, where n_r are uniformly randomly drawn from the interval [0, 1]. The signal is normalized by dividing the maximum magnitude of its entries. Then, M entries of the test signals are sampled uniformly at random. For each (R, M) pair, 100 Monte Carlo trials are conducted. Each trial is declared successful if $\|\boldsymbol{x} - \boldsymbol{y}\| / \|\boldsymbol{y}\| \le 10^{-3}$, where \boldsymbol{x} and \boldsymbol{y} are the true and reconstructed signals, respectively.

We plot in Figs. 1 and 2 the rate of successful reconstruction of undamped and damped complex sinusoids, respectively. The black and white region indicate a 0% and 100% of successful reconstruction, respectively, and a gray region between 0% and 100%. The top four plots in Fig. 1 present the recovery phase transitions where no separation of the frequencies is imposed, while the bottom four plots present the recovery phase

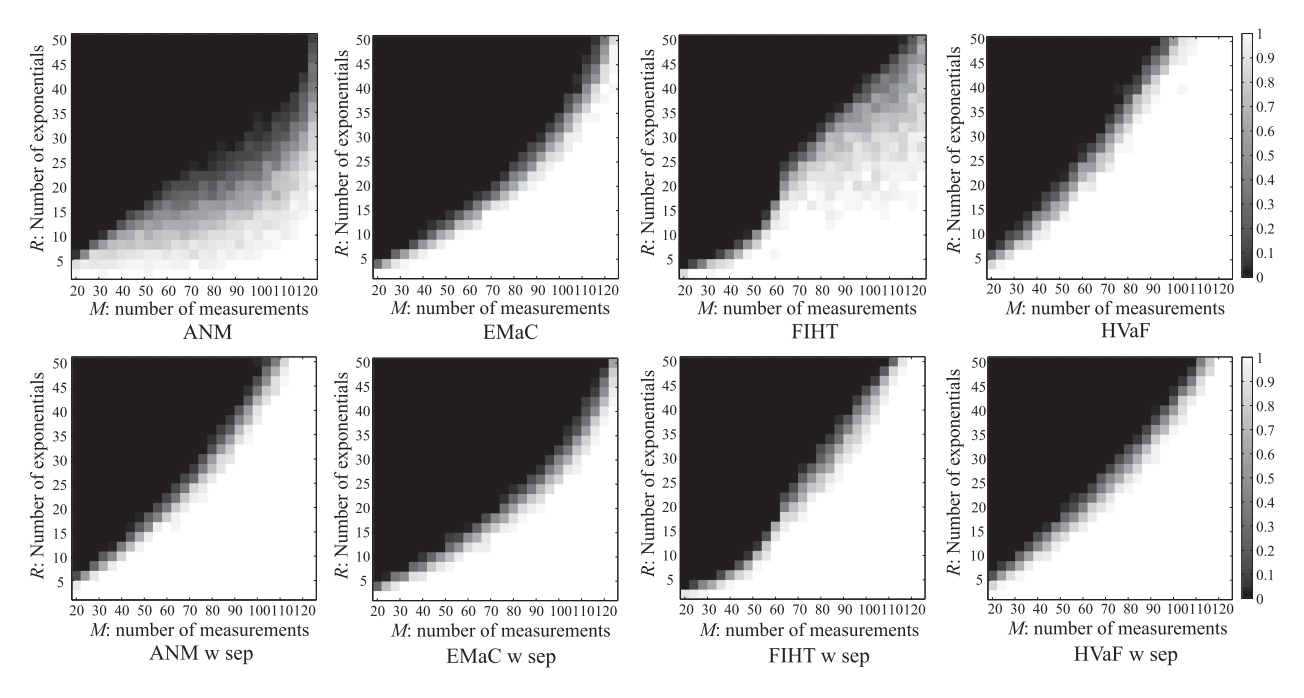


Fig. 1. Phase transition of successful reconstruction on undamped signals. Top: no restriction on frequencies of test signals; Bottom: wrap-around distances between frequencies are at least 1.5/(2N-1). The length of the test signal 2N-1 is 127.

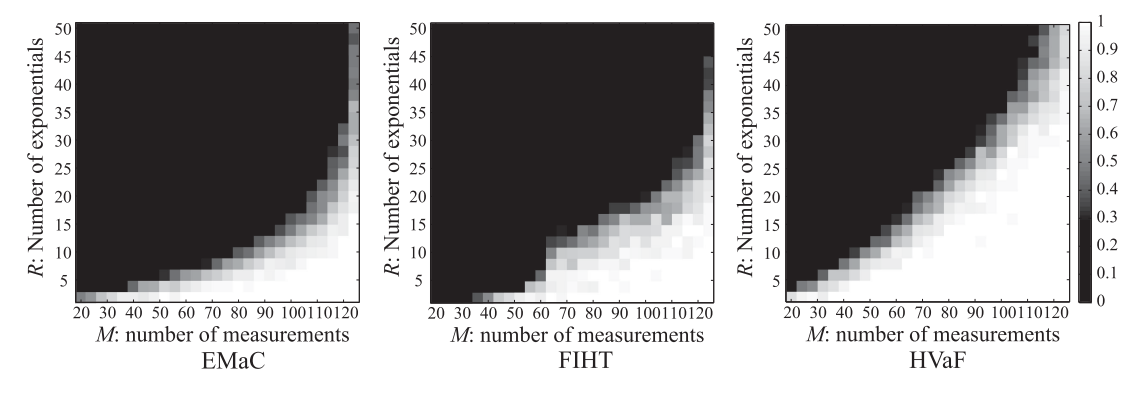


Fig. 2. Phase transition of successful reconstruction on damped signals. The comparison with ANM is ignored since it is still unknown how to extend ANM to recover damped signals. The length of the test signal 2N-1 is 127.

transitions where the wrap-around distances between the randomly drawn frequencies are greater than 1.5/(2N-1).

Fig. 1 shows the empirical phase transitions of undamped complex sinusoid recovery for the four compared algorithms. The phase transition boundary of HVaF is significantly higher than ANM, EMaC and FITH when no separation is imposed on frequencies, implying that, for a fixed number of exponentials, HVaF requires a smaller number of measurements for successful reconstruction. While the frequencies of test signals are separated, the phase transition boundaries of ANM and HVaF are similar, slightly higher than FIHT and EMaC. Moreover, the performance of ANM and FIHT degrades severely when the separation condition is not met, while EMaC and HVaF can still achieve good performance. Therefore, HVaF and EMaC are less sensitive to the separation requirement. It is worth mentioning that the required separation condition cannot guarantee to be satisfied in practice when the number of components R is relatively high.

Fig. 2 illustrates the empirical phase transitions of damped complex sinusoid recovery for EMaC, FIHT and HVaF. This type of signals arise in NMR spectroscopy [6]. The comparison with ANM is ignored since it is still unknown how to extend ANM to recover damped signals. Fig. 2 indicates that the phase transition of HVaF is much higher than EMaC and FIHT.

We further evaluate the reconstruction performance in terms of parameter estimation. In particular, we conduct the parameter estimation on the signal with small frequency separation, considering it is still challenging in this case to retrieve true parameters through reconstructions. A synthetic experiment is conducted on the signal with 5 peaks, as shown in Fig. 3 and ESPRIT [52], [53] is used to estimate frequencies and amplitudes of the reconstructed signals. The simulated signal includes two types of frequency separations, 0.5/(2N-1) and 1.5/(2N-1). The top and bottom three plots in Fig. 3 present the estimation of signals recovered from 50 and 25 samples, respectively.

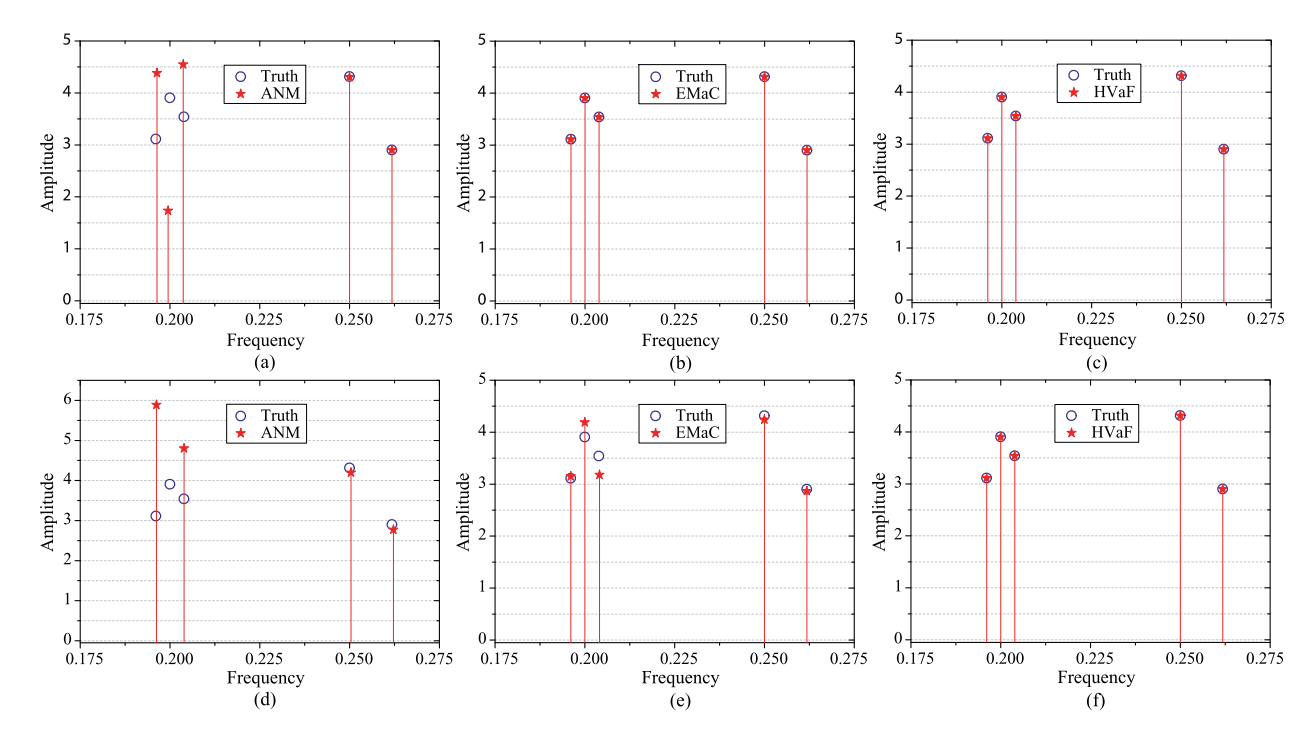


Fig. 3. Parameter estimation of undamped signal recovery. (a), (b) and (c) are the estimation of recovery from 50 measurements, and (d), (e) and (f) are the estimation of recovery from 25 measurements. The synthetic data is undamped complex exponential signal with 127 entries and 5 peaks. The frequencies of peaks are 0.2 - 0.5/127, 0.2, 0.2 + 0.5/127, 0.25, 0.25 + 1.5/127, implying that the frequency separation of the three peaks in the left side and the two peaks in the right side are 0.5/(2N-1) and 1.5/(2N-1), respectively. In addition, one peak is not drawn in (d) since its estimated frequency retrieved from ANM reconstruction is beyond the scale of horizontal axis. Besides, estimation results for FIHT are omitted since the algorithm is not convergent in this specific experiment. Here ρ in HVaF is 1.01.

Figs. 3(a) and (d) show that the amplitudes of the three peaks on the left side, where the frequency separation is 0.5/(2N-1), are estimated much worse than these of the two peaks on the right side, where the frequency separation is 1.5/(2N-1). It is observed that the true parameters with small frequency separation are not retrieved from ANM reconstruction. Figs. 3(b) and (e) show that the parameters with small frequency separation can be estimated accurately through EMaC reconstruction from 50 measurements, while estimation error increases when the number of measurements decreases to 25, implying that a relatively high sampling rate is necessary for EMaC to retrieve true parameters. It is observed from Fig. 3(c) and (f) that HVaF presents accurate parameter estimations in the case of small frequency separation and low sampling rate.

We further conduct 100 Monte Carlo trials of parameter estimation for the synthetic signal in Fig. 3 and each trial is declared successful if $\sqrt{\sum_{r=1}^R \left(\hat{f}_r - f_r\right)^2}/\sqrt{\sum_{r=1}^R f_r^2} \le 10^{-3}$ and $\sqrt{\sum_{r=1}^R \left(|\hat{c}_r| - |c_r|\right)^2}/\sqrt{\sum_{r=1}^R |c_r|^2} \le 10^{-3}$ are simultaneously satisfied, where \hat{f} and \hat{c}_r are the estimated frequency and amplitude of the true f_r and c_r . Fig. 4 shows that HVaF achieves higher success rate of parameter estimation than ANM and FIHT when frequency separation is small. Compared with EMaC, HVaF requires less measurements to obtain successful parameter estimation.

Fig. 5 evaluates the effect of preset number of exponentials R on reconstruction. It is observed that HVaF can always achieve high success rate as \hat{R} increases from 20 to 64, while the exact number of exponentials is 20. This observation indicates that

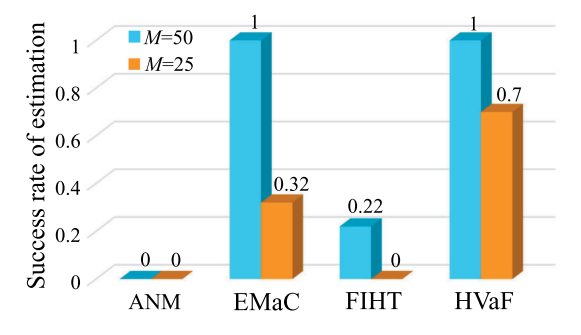


Fig. 4. Success rate of parameter estimation of undamped signal recovery. The success rate is calculated over 100 Monte Carlo trials.

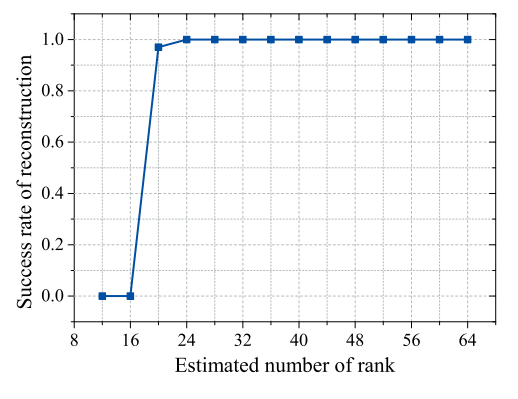


Fig. 5. The success rate of reconstructions versus estimated rank of HVaF. The exact number of exponentials R is 20 and the number of measurements M is 90.

TABLE I
COMPARISONS OF EMPIRICAL COMPUTATIONAL TIME (SEC)

ANM	EMaC	FIHT	HVaF ($\hat{R}=10$)	HVaF ($\hat{R} = 30$)	HVaF ($\hat{R} = 50$)
5.05	54.87	0.16	21.16	168.94	292.77

Note: The synthetic undamped signal consists of 10 peaks. The length of the signal is 127 and the number of measurements is 64. The computational time is computed by averaging 100 Monte Carlo trials. The numerical experiments are conducted on a Dell PC running Windows 10 operating system with Intel Core i5 4570 CPU and 8-GB RAM.

HVaF may have great potential to reconstruct a signal even in the case that a much larger \hat{R} than R is given. Thus, flexible setting of \hat{R} is possible for the proposed HVaF.

Table I shows the average computational time of each method. We can see the large estimated rank \hat{R} in HVaF will result in the long computational time. Therefore, \hat{R} should not be overrated too much considering the computational cost, though the reconstruction results will not be degraded.

B. Real NMR Spectroscopy Data

NMR spectroscopy plays an important role in studying structure, dynamics and interactions of biopolymers in chemistry and biology. The non-uniform sampling is popular to reduce the number of measurements [6], [54]–[59] due to the long duration of spectroscopy experiment.

The time domain signal of NMR is usually modelled as a superposition of damped complex sinusoids [6], [60]. The efficiency of LRHM has been verified in NMR spectroscopy [6], showing advantages in recovering broad peaks over l_1 norm minimization on the spectrum [56]–[59]. However, LRHM needs a relatively high sampling rate, for example 35% for the following NMR spectrum [6], to obtain a reliable reconstruction. In this section, we will compare HVaF with LRHM in recovering realistic biological NMR spectroscopy data with a lower sampling rate. The comparisons with ANM and FIHT are ignored, since ANM is not available in recovering damped signals and the number of exponentials in realistic NMR spectroscopy cannot be exactly estimated for FIHT.

Here we apply HVaF to recover a $^1\mathrm{H}^{-15}\mathrm{N}$ spectrum from Poisson-gap [54] non-uniformly sampled time-domain data. The data compose a matrix \boldsymbol{X} with the size 255×116 , where columns and rows indicate $^{15}\mathrm{N}$ and $^1\mathrm{H}$ dimensions, respectively. According to the principle of NMR experiments, each column of the spectrum is non-uniformly sampled and can be reconstructed individually. The spectrum is normalized by dividing the maximum magnitude of its entries as pre-processing.

Fig. 6 shows the reconstructed spectra using a 22% sampling rate, indicating that HVaF leads to a more faithful recovery of the full sampled spectra than LRHM. As marked by the arrows in Fig. 6, some peaks are underestimated severely in LRHM reconstruction but not in HVaF. Here we compute the Relative Least Normalized Error (RLNE) by

$$\|X - Y\|_F / \|Y\|_F,$$
 (38)

where X is the reconstructed 2D spectrum and Y is the fully sampled 2D spectrum with noise. The reconstruction errors by HVaF and LRHM are 0.1036 and 0.1127, respectively. But note

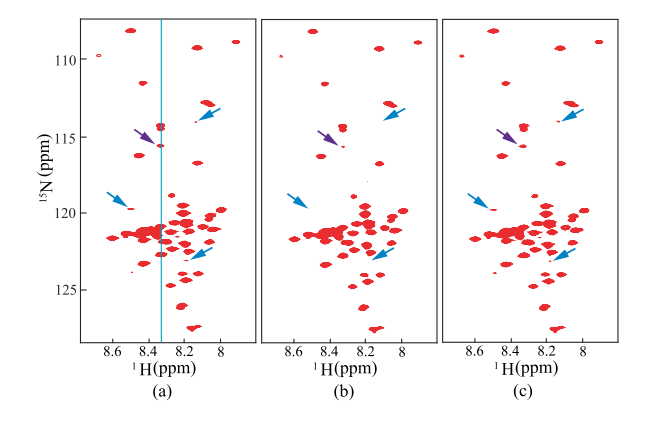


Fig. 6. The NMR spectra recovery under 22% non-uniform sampling. (a) Fully sampled spectrum; (b) and (c) are the reconstructed spectra by LRHM and HVaF, respectively. The ppm denotes parts per million by frequency, the unit of chemical shift.

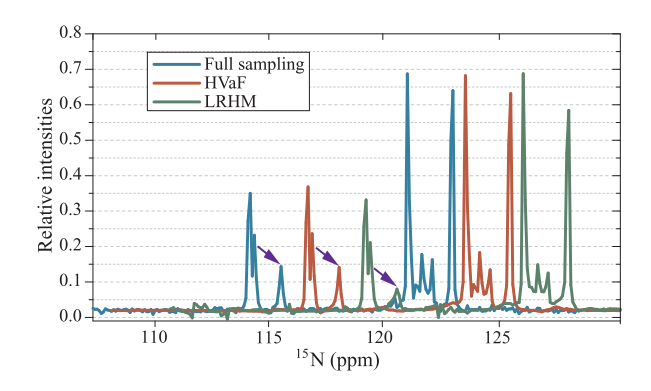


Fig. 7. One column of the reconstructed spectra by LRHM and HVaF. The column spectrum is along the dimension of $^{15}\,\mathrm{N}$ and are located at 8.35 ppm of the dimension of $^{1}\,\mathrm{H}$. Note: The 1D spectrum are shifted for better visualization.

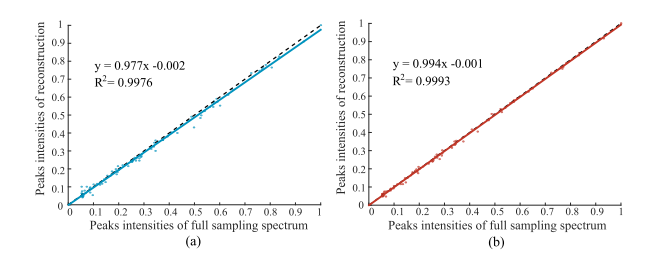


Fig. 8. Peak intensities correlation between the full sampled spectrum and the reconstructed spectrum. (a) and (b) are correlation evaluation for LRHM and HVaF, respectively. Note that the notation R^2 denotes Pearsons linear correlation coefficient of fitted curve. The closer the value of R^2 gets to 1, the stronger the correlation between the full sampled spectrum and the reconstructed spectrum is. Here, 83 peaks are extracted and their intensities, obtained by finding the local maximum within a spectrum region (three by three points), are adopted in correlation analysis. Spectrum intensities that are smaller than the noise level, 0.05 in this case, are treated as noise and will not be plotted or used for correlation analysis.

that the reconstruction errors here are not very conclusive, since the fully sampled spectrum is noisy. Therefore we further present qualitative results and peak corrections. Fig. 7 illustrates one column of the reconstructed spectra. It is observed that HVaF achieves a reliable reconstruction while LRHM weakens the marked peak and introduces some artifact peaks. Fig. 8 further presents that the HVaF achieve higher accuracy of peak

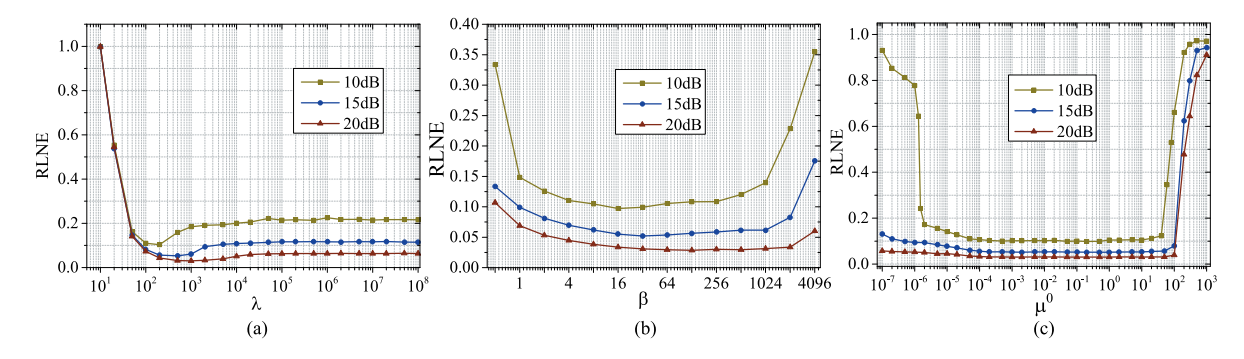


Fig. 9. RLNE versus parameters (a) λ , (b) β and μ^0 under different noise levels. In (a), β and μ^0 are 32 and 0.05, respectively; In (b), the λ is set as 200, 500 and 1000 under noise levels 10 dB, 15 dB and 20 dB, respectively. μ^0 is 0.05; In (c), the setting of λ is the same with that in (b) and β is 32.

intensities. This observation is consistent with Fig. 2 showing that a higher success rate is obtained with the proposed approach under the same number of measurements. The advantage of HVaF over LRHM implies a more significant reduction in measurement time and thus HVaF will be valuable for the biological NMR applications.

V. DISCUSSIONS

A. Parameter Setting in the Model and Algorithm

The proposed method includes the parameter λ in the mathematical model as well as β and μ^0 in the numerical algorithm. Fig. 9 shows the impact of λ , β and μ^0 on the reconstruction error, respectively. The synthetic signal in these experiments consists of 5 complex exponentials and the number of observed entries is 64. The measurements are corrupted by the noise

$$e = \sigma \cdot \|\mathcal{P}_{\Omega}(y)\| \cdot \frac{w}{\|w\|},$$
 (39)

where $\|\cdot\|$ is ℓ_2 -norm, \boldsymbol{y} is the true signal, the entries of \boldsymbol{w} are i.i.d. standard Gaussian random variables and σ is referred to as the noise level. The σ is set as $10^{-0.5}$, $10^{-0.75}$ and 10^{-1} in experiments, and the corresponding signal-to-noise ratios (SNR), is 10 dB, 15 dB and 20 dB, where SNR is computed by

$$SNR = -10 \log_{10} \frac{\|e\|^2}{\|\mathcal{P}_{\Omega}(y)\|^2}.$$
 (40)

Fig. 9(a) indicates that the available range, leading to the reconstruction error RLNE ≤ 0.1 , turns narrowed when the noise level increases. The optimal λ , which produces the lowest reconstruction error, generally decreases as the noise level increases. For example, as shown in Fig. 9(a), the optimal λ is 200, 500 and 1000 for noise levels of 10 dB, 15 dB and 20 dB, respectively. This means that a smaller λ should be set for a higher noise level. From Figs. 9(b) and 9(c), we can see the reconstruction error is steady over a large range of choice of β and μ^0 under different noise levels.

B. Parameter Estimation of Damped Signal Recovery

Experiments on parameter estimation of damped signal recovery are conducted here. It is observed that all of the compared methods, EMaC, FIHT and HVaF, achieve accurate parameter estimation if sufficient number of samples, 60 samples in the simulation, are available. However, the performance of EMaC degrades severely when the number of samples is reduced to 30 as shown in Table II, while HVaF still obtains good performance. This observation implies that HVaF requires fewer samples to achieve accurate estimation than EMaC.

C. Frequency Identifiability

The results shown in Fig. 1 imply that the proposed method achieved a better signal reconstruction performance when frequencies were closer. A possible reason is that HVaF favors deciding that there is a single one frequency component in the case that two frequencies are extremely close with each other.

This guess is further confirmed by the results shown in Table III, indicating that the method is not able to distinguish frequency components that are close together in the missing data recovery. Table III shows an experiment on two-component signal reconstruction. Here we consider two cases of frequency separations between the two frequency components, 0.01/(2N-1)and 1.5/(2N-1). It is observed that, to obtain low reconstruction error (RLNE $\leq 10^{-3}$), the signal with frequency separation 0.01/(2N-1) requires less measurements than the signal with separation 1.5/(2N-1). Spectral parameter estimation on the reconstructed signal shows that, the original two close peaks are synthesized together since the magnitude of one spectral peak has been reduced from 0.66 to 1.4×10^{-4} . This observation implies that the rank of the Hankel matrix in the iterative reconstruction may be reduced to 1. Thus, a small number of measurements is possible in the reconstruction.

However, our method is intended to reconstruct the missing data rather than estimate spectral parameters, and thus aims to obtain a low signal reconstruction error. In summary, the proposed HVaF has shown much better missing data reconstruction performance than the compared methods. The HVaF still has limitation on preserving very close frequencies in the case of missing data, which is always very challenging and will be a valuable future work.

Peak index	True parameters	Parameter estimation errors		
1 cak midex	(c_r , f_r, τ_r)	EMaC	HVaF $(10^{-6}, 10^{-8}, 10^{-4})$	
1	0.5145, 0.1532, 26.47	0.2097, 0.1603, 26.25	2.8, 1.4, 1.1	
2	0.6623, 0.3135, 35.63	0.3615, 0.1594, 0.437	2.3, 2.0, 0.4	
3	0.7253, 0.4716, 48.78	0.2157, 0.0001, 14.34	2.7, 0.2, 1.3	
4	0.7825, 0.6124, 61.51	0.2060, 0.0003, 19.63	0.7, 0.5, 0.4	
5	0.9872, 0.7831, 81.50	0.1531, 0.0003, 14.75	1.5, 0.3, 1.2	

TABLE II
PARAMETER ESTIMATION COMPARISONS OF DAMPED SIGNAL RECOVERY

Note: The synthetic signal with 5 peaks is generated by $y_k = \sum_{r=1}^5 c_r \, e^{(i\, 2\pi\, f_r\, -\tau_r\,)\, k}, \, k=1,\ldots,127$, where c_r , f_r and τ_r denote the complex amplitude, frequency and damping factor of the rth peak, respectively. The number of samples is 30. ESPRIT [52], [53] is used to estimate the parameters of the reconstructed signals. The results of FIHT are omitted since FIHT is not convergent in this case.

TABLE III
PARAMETER ESTIMATION UNDER DIFFERENT FREQUENCY SEPARATIONS

Peak index	True parameters f_r , $ c_r $		Estimated \hat{f}_r , $ \hat{c}_r $ $(M=8)$		Estimated \hat{f}_r , $ \hat{c}_r $ $(M=12)$	
1 cak macx	0.01/(2 <i>N</i> -1)	1.5/(2 <i>N</i> -1)	0.01/(2N-1)	1.5/(2 <i>N</i> -1)	0.01/(2N-1)	1.5/(2 <i>N</i> -1)
1	0.3000, 0.5100	0.3000, 0.5100	0.3000, 1.1681	0.2992, 0.4346	0.3000, 1.1672	0.3000, 0.5100
2	0.3001, 0.6600	0.3118, 0.6600	$0.2981, 1.4 \times 10^{-4}$	0.3328, 0.3550	$0.3004, 9.8 \times 10^{-5}$	0.3118, 0.6600
Reconstruction error (RLNE)			3.7×10^{-5}	0.2163	1.0×10^{-5}	5.6×10^{-6}

Note: The synthetic signal with 2 peaks is generated by $y_k = \sum_{r=1}^2 c_r e^{2\pi i f_r k}$, $k = 1, \dots, 127$, where c_r and f_r denote the complex amplitude, and frequency of the rth peak, respectively. ESPRIT [52], [53] is used to estimate the parameters of the reconstructed signals.

VI. CONCLUSIONS

A new approach, HVaF, is proposed to reconstruct the exponential signal by exploiting the Vandermonde factorization of the Hankel matrix formed by the signal. To implement HVaF, a numerical algorithm was developed and the sequence convergence were analysed. Experiments on synthetic data demonstrated that HVaF achieves higher empirical phase transition than nuclear-norm based minimization and fast iterative hard thresholding algorithm. Another advantage over state-of-the-art atomic norm minimization and fast iterative hard thresholding algorithm was empirically observed that HVaF can reconstruct signals with small frequency separation. The proposed method was further verified on reconstruction of fast sampled NMR spectroscopy, implying that HVaF may serve as an effective method for fast sampling of NMR spectroscopy in chemistry and biology.

For future work, it is of great interest to develop more efficient numerical methods to solve HVaF when the datasets are huge. In addition, we can also introduce rank minimization [61], truncated nuclear norm [62], or weighted nuclear norm [63] which may achieve extra improvements in reconstruction, e.g., better recovery of low intensity spectral peaks, since the low rank property can be better approximated than the commonly used nuclear norm.

APPENDIX

A. The Closed-Form Solutions of U and V

The closed-form solution of U can be obtained by solving (25). According to definitions of the operators \mathcal{R} and \mathcal{R}^* , we obtain $\mathcal{R}^*\mathcal{R}x = w \odot x$, where w is a vector and its k-th element w_k is the number of elements in k-th anti-diagonal of the Hankel

matrix $\mathcal{R}\boldsymbol{x}$. Here \odot denotes Hadamard product. In addition, according to definitions of \mathcal{Q} and \mathcal{Q}_r^* , we have $[\mathcal{Q}_r^*\mathcal{Q}_r\boldsymbol{X}]_{(:,k)} = \begin{cases} \boldsymbol{X}_{(:,r)} & k=r, \\ 0 & k\neq r. \end{cases}$ Hence, for $\boldsymbol{X} \in \mathbb{C}^{N \times N}$, by combination we

$$\sum_{r=1}^{\hat{R}} \mathcal{Q}_r^* \mathcal{R}^* \mathcal{R} \mathcal{Q}_r \boldsymbol{X} = \boldsymbol{T} \odot \boldsymbol{X},$$

where T is a constant matrix and each column of T is w. Therefore, we rewrite (25) as

$$\mu^k \mathbf{T} \odot \mathbf{U} + \beta \mathbf{U} (\mathbf{V}^k)^T \operatorname{conj}(\mathbf{V}^k) = \mathbf{Y}.$$

where the right term of (25) is denoted by Y. Obviously, we can obtain the closed-form solution of each row of U by

$$\mu^k \boldsymbol{U}_{(r,:)} \boldsymbol{T}_r + \beta \boldsymbol{U}_{(r,:)} (\boldsymbol{V}^k)^T \operatorname{conj}(\boldsymbol{V}^k) = \boldsymbol{Y}_{(r,:)},$$

and its solution is

$$\boldsymbol{U}_{(r,:)} = \boldsymbol{Y}_{(r,:)} (\mu^k \boldsymbol{T}_r + \beta (\boldsymbol{V}^k)^T \operatorname{conj}(\boldsymbol{V}^k))^{-1}.$$

where T_r is a diagonal matrix and its main diagonal is $T_{(r,:)}$. Therefore we can update U by updating each row and it is similar to update V.

ACKNOWLEDGMENT

The authors would like to thank Y. Chi for sharing EMaC codes for comparisons and Vladislav and Maxim for sharing the NMR data used in paper [6]. J. Ying would like to thank B. B. Haro and Q. Li for helpful discussions related to this paper. The authors also appreciate reviewers for their constructive comments.

REFERENCES

- [1] J. A. Tropp, J. N. Laska, M. F. Duarte, J. K. Romberg, and R. G. Baraniuk, "Beyond Nyquist: Efficient sampling of sparse bandlimited signals," *IEEE Trans. Inf. Theory*, vol. 56, no. 1, pp. 520–544, Jan. 2010.
- [2] D. Nion and N. D. Sidiropoulos, "Tensor algebra and multidimensional harmonic retrieval in signal processing for MIMO radar," *IEEE Trans. Signal Process.*, vol. 58, no. 11, pp. 5693–5705, Nov. 2010.
- [3] C. Qian, L. Huang, M. Cao, J. Xie, and H. C. So, "PUMA: An improved realization of MODE for DOA estimation," *IEEE Trans. Aerosp. Electron. Syst.*, vol. 53, no. 5, pp. 2128–2139, Oct. 2017.
- [4] L. Schermelleh, R. Heintzmann, and H. Leonhardt, "A guide to superresolution fluorescence microscopy," *J. Cell Biol.*, vol. 190, no. 2, pp. 165– 175, 2010.
- [5] Z.-P. Liang, E. M. Haacke, and C. W. Thomas, "High-resolution inversion of finite fourier transform data through a localised polynomial approximation," *Inverse Problems*, vol. 5, no. 5, pp. 831–848, 1989.
- [6] X. Qu, M. Mayzel, J.-F. Cai, Z. Chen, and V. Orekhov, "Accelerated NMR spectroscopy with low-rank reconstruction," *Angew. Chemie-Int.* Ed., vol. 54, no. 3, pp. 852–854, 2015.
- [7] J. Ying et al., "Hankel matrix nuclear norm regularized tensor completion for N-dimensional exponential signals," *IEEE Trans. Signal Process.*, vol. 65, no. 14, pp. 3702–3717, Jul. 2017.
- [8] H. M. Nguyen, X. Peng, M. N. Do, and Z.-P. Liang, "Denoising MR spectroscopic imaging data with low-rank approximations," *IEEE Trans. Biomed Eng.*, vol. 60, no. 1, pp. 78–89, Jan. 2013.
- [9] H. Lu et al., "Low rank enhanced matrix recovery of hybrid time and frequency data in fast magnetic resonance spectroscopy," *IEEE Trans. Biomed. Eng.*, vol. 65, no. 4, pp. 809–820, Apr. 2018.
- [10] D. Guo, H. Lu, and X. Qu, "A fast low rank Hankel matrix factorization reconstruction method for non-uniformly sampled magnetic resonance spectroscopy," *IEEE Access*, vol. 5, pp. 16033–16039, 2017.
- [11] S. Ye, E. Aboutanios, D. S. Thomas, and J. M. Hook, "Localised high resolution spectral estimator for resolving superimposed peaks in NMR signals," *Signal Process.*, vol. 130, pp. 343–354, 2017.
- [12] E. J. Candès, J. Romberg, and T. Tao, "Robust uncertainty principles: exact signal reconstruction from highly incomplete frequency information," *IEEE Trans. Inf. Theory*, vol. 52, no. 2, pp. 489–509, Feb. 2006.
- [13] Y. Chi, L. L. Scharf, A. Pezeshki, and A. R. Calderbank, "Sensitivity to basis mismatch in compressed sensing," *IEEE Trans. Signal Process.*, vol. 59, no. 5, pp. 2182–2195, May 2011.
- [14] V. Chandrasekaran, B. Recht, P. A. Parrilo, and A. S. Willsky, "The convex geometry of linear inverse problems," *Found. Comput. Math.*, vol. 12, no. 6, pp. 805–849, 2012.
- [15] G. Tang, B. N. Bhaskar, P. Shah, and B. Recht, "Compressed sensing off the grid," *IEEE Trans. Inf. Theory*, vol. 59, no. 11, pp. 7465–7490, Nov. 2013.
- [16] E. J. Candès and C. Fernandez-Granda, "Towards a mathematical theory of super-resolution," *Commun. Pure Appl. Math.*, vol. 67, no. 6, pp. 906–956, 2014.
- [17] Y. Chi and Y. Chen, "Compressive two-dimensional harmonic retrieval via atomic norm minimization," *IEEE Trans. Signal Process.*, vol. 63, no. 4, pp. 1030–1042, Feb. 2015.
- [18] Z. Yang and L. Xie, "On gridless sparse methods for line spectral estimation from complete and incomplete data," *IEEE Trans. Signal Process.*, vol. 63, no. 12, pp. 3139–3153, Jun. 2015.
- [19] W. Xu, J.-F. Cai, K. V. Mishra, M. Cho, and A. Kruger, "Precise semidefinite programming formulation of atomic norm minimization for recovering d-dimensional (d ≥ 2) off-the-grid frequencies," in Proc. IEEE Inf. Theory Appl. Workshop, 2014, pp. 1–4.
- [20] J. Fang, J. Li, Y. Shen, H. Li, and S. Li, "Super-resolution compressed sensing: An iterative reweighted algorithm for joint parameter learning and sparse signal recovery," *IEEE Signal Process. Letters*, vol. 21, no. 6, pp. 761–765, Jun. 2014.
- [21] M. F. D. Costa and W. Dai, "Low dimensional atomic norm representations in line spectral estimation," in *Proc. IEEE Int. Symp. Inf. Theory*, 2017, pp. 226–230.
- [22] M. Fazel, T. K. Pong, D. Sun, and P. Tseng, "Hankel matrix rank minimization with applications to system identification and realization," SIAM J. Matrix Anal. Appl., vol. 34, no. 3, pp. 946–977, 2013.
- [23] I. Markovsky and K. Usevich, "Structured low-rank approximation with missing data," SIAM J. Matrix Anal. Appl., vol. 34, no. 2, pp. 814–830, 2013.
- [24] F. Andersson, M. Carlsson, J.-Y. Tourneret, and H. Wendt, "A new frequency estimation method for equally and unequally spaced data," *IEEE Trans. Signal Process.*, vol. 62, no. 21, pp. 5761–5774, Nov. 2014.

- [25] Y. Chen and Y. Chi, "Robust spectral compressed sensing via structured matrix completion," *IEEE Trans. Inf. Theory*, vol. 60, no. 10, pp. 6576– 6601, Oct. 2014.
- [26] J.-F. Cai, X. Qu, W. Xu, and G.-B. Ye, "Robust recovery of complex exponential signals from random Gaussian projections via low rank Hankel matrix reconstruction," *Appl. Comput. Harmonic Anal.*, vol. 41, no. 2, pp. 470–490, 2016.
- [27] K. Usevich and P. Comon, "Hankel low-rank matrix completion: Performance of the nuclear norm relaxation," *IEEE J. Sel. Topics Signal Process.*, vol. 10, no. 4, pp. 637–646, Jun. 2016.
- [28] J.-F. Cai, S. Liu, and W. Xu, "A fast algorithm for reconstruction of spectrally sparse signals in super-resolution," *Proc. SPIE*, vol. 9597, 2015, Art. no. 95970A.
- [29] I. Markovsky, "Recent progress on variable projection methods for structured low-rank approximation," Signal Process., vol. 96, pp. 406–419, 2014
- [30] J.-F. Cai, T. Wang, and K. Wei, "Fast and provable algorithms for spectrally sparse signal reconstruction via low-rank Hankel matrix completion," *Appl. Comput. Harmonic Anal.*, 2017. [Online]. Available: http://dx.doi.org/10.1016/j.acha.2017.04.004
- [31] J.-F. Cai, T. Wang, and K. Wei, "Spectral compressed sensing via projected gradient descent," 2017, arXiv:1707.09726.
- [32] J. P. Haldar, "Low-rank modeling of local k-space neighborhoods (LO-RAKS) for constrained MRI," *IEEE Trans. Med. Imag.*, vol. 33, no. 3, pp. 668–681, Mar. 2014.
- [33] G. Ongie and M. Jacob, "Off-the-grid recovery of piecewise constant images from few Fourier samples," *SIAM J. Imag. Sci.*, vol. 9, no. 3, pp. 1004–1041, 2016.
- [34] K. H. Jin, D. Lee, and J. C. Ye, "A general framework for compressed sensing and parallel MRI using annihilating filter based low-rank Hankel matrix," *IEEE Trans. Comput. Imag.*, vol. 2, no. 4, pp. 480–495, Dec. 2016.
- [35] P. J. Shin et al., "Calibrationless parallel imaging reconstruction based on structured low-rank matrix completion," Mag. Reson. Med., vol. 72, no. 4, pp. 959–970, 2014.
- [36] M. Vetterli, P. Marziliano, and T. Blu, "Sampling signals with finite rate of innovation," *IEEE Trans. Signal Process.*, vol. 50, no. 6, pp. 1417–1428, Jun. 2002.
- [37] P. L. Dragotti, M. Vetterli, and T. Blu, "Sampling moments and reconstructing signals of finite rate of innovation: Shannon meets strang-fix," *IEEE Trans. Signal Process.*, vol. 55, no. 5, pp. 1741–1757, May 2007.
- [38] B. B. Haro and M. Vetterli, "Sampling continuous-time sparse signals: A frequency-domain perspective," *IEEE Trans. Signal Process.*, vol. 66, no. 6, pp. 1410–1424, Mar. 2018.
- [39] T. Blu, P.-L. Dragotti, M. Vetterli, P. Marziliano, and L. Coulot, "Sparse sampling of signal innovations," *IEEE Signal Process. Mag.*, vol. 25, no. 2, pp. 31–40, Mar. 2008.
- [40] L. Condat and A. Hirabayashi, "Cadzow denoising upgraded: A new projection method for the recovery of dirac pulses from noisy linear measurements," Sampling Theory Signal Image Process., vol. 14, no. 1, pp. 17–47, 2015.
- [41] X. Qu, J. Ying, J.-F. Cai, and Z. Chen, "Accelerated magnetic resonance spectroscopy with Vandermonde factorization," in *Proc. 39th Ann. Int. Conf. IEEE Eng. Med. Biol. Soc.*, 2017, pp. 3537–3540.
- [42] T.-H. Chan, W.-K. Ma, C.-Y. Chi, and Y. Wang, "A convex analysis framework for blind separation of non-negative sources," *IEEE Trans. Signal Process.*, vol. 56, no. 10, pp. 5120–5134, Oct. 2008.
- [43] X. Fu, N. D. Sidiropoulos, and W.-K. Ma, "Power spectra separation via structured matrix factorization," *IEEE Trans. Signal Process.*, vol. 64, no. 17, pp. 4592–4605, Sep. 2016.
- [44] D. Geman and C. Yang, "Nonlinear image recovery with half-quadratic regularization," *IEEE Trans. Image Process.*, vol. 4, no. 7, pp. 932–946, Jul. 1995.
- [45] M. Nikolova and M. K. Ng, "Analysis of half-quadratic minimization methods for signal and image recovery," SIAM J. Sci. Comput., vol. 27, no. 3, pp. 937–966, 2005.
- [46] X. Qu, Y. Hou, F. Lam, D. Guo, J. Zhong, and Z. Chen, "Magnetic resonance image reconstruction from undersampled measurements using a patch-based nonlocal operator," *Med. Image Anal.*, vol. 18, no. 6, pp. 843– 856, 2014.
- [47] Z. Zhan, J.-F. Cai, D. Guo, Y. Liu, Z. Chen, and X. Qu, "Fast multiclass dictionaries learning with geometrical directions in MRI reconstruction," *IEEE Trans. Biomed. Eng.*, vol. 63, no. 9, pp. 1850–1861, Sep. 2016.
- [48] J.-F. Cai, E. J. Candès, and Z. Shen, "A singular value thresholding algorithm for matrix completion," SIAM J. Optim., vol. 20, no. 4, pp. 1956– 1982, 2010.

- [49] F. Shang, Y. Liu, and J. Cheng, "Tractable and scalable schatten quasinorm approximations for rank minimization," in *Proc. 19th Int. Conf.* Artif. Intell. Statist., 2016, pp. 2016–2022.
- [50] Z. Lin, M. Chen, and Y. Ma, "The augmented Lagrange multiplier method for exact recovery of corrupted low-rank matrices," Univ. Illinois, Urbana-Champaign, Champaign, IL, USA, Tech. Rep. UILU-ENG-09-2215, 2009.
- [51] M. Grant and S. Boyd, "CVX: MATLAB software for disciplined convex programming, version 2.1," 2014. [Online]. Available: http://cvxr.com/cvx
- [52] R. Roy and T. Kailath, "ESPRIT-estimation of signal parameters via rotational invariance techniques," *IEEE Trans. Acoust., Speech, Signal Process.*, vol. 37, no. 7, pp. 984–995, Jul. 1989.
- [53] P. Stoica and R. L. Moses, Spectral Analysis of Signals. Upper Saddle River, NJ, USA: Prentice-Hall, 2005.
- [54] S. G. Hyberts, K. Takeuchi, and G. Wagner, "Poisson-gap sampling and forward maximum entropy reconstruction for enhancing the resolution and sensitivity of protein NMR data," *J. Amer. Chemical Soc.*, vol. 132, no. 7, pp. 2145–2147, 2010.
- [55] V. Y. Orekhov and V. Jaravine, "Analysis of non-uniformly sampled spectra with multi-dimensional decomposition," *Prog. Nucl. Mag. Reson. Spectrosc.*, vol. 59, no. 3, pp. 271–292, 2011.
- [56] X. Qu, X. Cao, D. Guo, and Z. Chen, "Compressed sensing for sparse magnetic resonance spectroscopy," in *Proc. 18th Sci. Meeting Int. Soc. for Mag. Resonance Med.*, 2010, p. 3371.
- [57] K. Kazimierczuk and V. Y. Orekhov, "Accelerated NMR spectroscopy by using compressed sensing," *Angew. Chemie-Int. Ed.*, vol. 123, no. 24, pp. 5670–5673, 2011.
- [58] D. J. Holland, M. J. Bostock, L. F. Gladden, and D. Nietlispach, "Fast multidimensional NMR spectroscopy using compressed sensing," *Angew. Chemie-Int. Ed.*, vol. 123, no. 29, pp. 6678–6681, 2011.
- [59] X. Qu, D. Guo, X. Cao, S. Cai, and Z. Chen, "Reconstruction of self-sparse 2D NMR spectra from undersampled data in the indirect dimension," *Sensors*, vol. 11, no. 9, pp. 8888–8909, 2011.
- [60] J. C. Hoch and A. S. Stern, NMR Data Processing. Hoboken, NJ, USA: Wiley, 1996.
- [61] M. Le Pendu, X. Jiang, and C. Guillemot, "Light field inpainting propagation via low rank matrix completion," *IEEE Trans. Image Process.*, vol. 27, no. 4, pp. 1981–1993, Apr. 2018.
- [62] T.-H. Oh, Y.-W. Tai, J.-C. Bazin, H. Kim, and I. S. Kweon, "Partial sum minimization of singular values in robust PCA: Algorithm and applications," *IEEE Trans. Pattern Anal. Mach. Intell.*, vol. 38, no. 4, pp. 744–758, Apr. 2016.
- [63] D. Guo and X. Qu, "Improved reconstruction of low intensity magnetic resonance spectroscopy with weighted low rank Hankel matrix completion," *IEEE Access*, vol. 6, pp. 4933–4940, 2018.



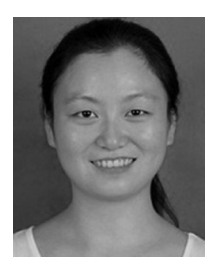
Jiaxi Ying received the B.S. degree from the School of Science, Nanjing University of Science and Technology, Nanjing, China, in 2012 and the M.S. degree from the Department of Electronic Science, Xiamen University, Xiamen, China, in 2017. Since then, he has been a Research Assistant with the Department of Mathematics, Hong Kong University of Science and Technology, Clear Water Bay, Hong Kong. His research interests include optimization, statistical signal processing, information theory, harmonic analysis, and their applications to machine learning, med-

ical imaging, and inverse problems.



Jian-Feng Cai received the B.S. and M.S. degrees in computational mathematics from Fudan University, Shanghai, China, in 2000 and 2004, respectively, and the Ph.D. degree in mathematics from Chinese University of Hong Kong, Shatin, Hong Kong, in 2007. He is currently an Associate Professor with the Department of Mathematics, Hong Kong University of Science and Technology, Clear Water Bay, Hong Kong. Before taking his position at HKUST, he was with National University of Singapore (2007–2009), University of California, Los Angeles (2009–2011),

and University of Iowa (2011–2015). His research interests include the design and analysis of efficient algorithms for real-world problems (e.g., data analysis, signal/image processing, machine learning), using tools from computational harmonic analysis, approximation theory, numerical linear algebra, optimization, and probability. He has been named as a Highly Cited Researcher in Mathematics by Clarivate Analytics in 2017.



Di Guo received the B.S. and Ph.D. degrees in communication engineering from Xiamen University, Xiamen, China, in 2005 and 2012, respectively. She is currently an Associate Professor with the Department of Computer Science and Technology, Xiamen University of Technology, Xiamen, China. From 2009 to 2011, she was a Visiting Scientist with the Department of Electrical Engineering, University of Washington, Seattle, WA, USA. Her research interests include signal and image processing, and their applications in biomedical engineering, wireless sen-

sor networks, and Internet of things. She won the IBM Distinguished Student Award in 2012.



Gongguo Tang (S'09–M'11) received the Ph.D. degree in electrical engineering from Washington University in St. Louis, St. Louis, MO, USA, in 2011. He was a Postdoctoral Research Associate with the Department of Electrical and Computer Engineering, University of Wisconsin-Madison, Madison, WI, USA, in 2013.

He is currently an Assistant Professor with the Colorado School of Mines, Golden, CO, USA. His research interests include using convex and non-convex optimization methods to model and solve problems

in signal processing and machine learning, with focus on designing optimization procedures that come with theoretical performance guarantees and are scalable to large data sets.



Zhong Chen received the B.S. and M.S. degrees in radio physics, and the Ph.D. degree in physical chemistry from Xiamen University, Xiamen, China, in 1985, 1988, and 1993, respectively. In June 1995, he joined Xiamen University as an Associate Professor and was appointed as the Director of the Magnetic Resonance Center. From July 1998 to December 2000, he was a Visiting Associate Professor with the University of Rochester, USA. Since 2007, he has been a Distinguished Professor of Minjiang Scholar. He was a Vice-President of the College of Physics

and Electromchanical Engineering from 2003 to 2017, and has been an Executive Vice-President of the College of Electronic Science and Technology from 2017, both in Xiamen University. His research interests are centered on nuclear magnetic resonance techniques and applications. He has authored or coauthored more than 300 papers and 48 patents (including 2 U.S. patents). He is on the editorial board of the *Journal of Magnetic Resonance* and many other journals.



Xiaobo Qu received the B.S. and Ph.D. degrees in communication engineering from Xiamen University, Xiamen, China, in 2006 and 2011, respectively. He is currently an Associate Professor with the Department of Electronic Science, Research Center of Magnetic Resonance and Medical Imaging, and Research Center for Molecular Imaging and Translational Medicine in the same university. From 2009 to 2011, he was a visiting scholar with the Department of Electrical and Computer Engineering, University of Illinois at Urbana-Champaign. Since 2012, he has

been a Faculty Member with Xiamen University. From July 2014 to September 2014, he was the Visiting Scientist with Swedish NMR Centre, University of Gothenburg, Sweden. His research interests include magnetic resonance imaging and spectroscopy, signal and image representations, computational imaging, machine learning, and artificial intelligence. He has been a member of ISMRM, IEEE EMBS, and SPS. He is the Associate Editor of the IEEE TRANSACTIONS ON COMPUTATIONAL IMAGING, Section Editor of BMC Medical Imaging, and on the editorial board of Quantitative Imaging in Medicine and Surgery. He was the recipient of the E. K. Zavoisky Stipend (2014, 2016, 2018) of ISMRM Scientific Meeting, Swedish Wenner-Gren Fellowship (2014), Distinguished Young Scholar Award in Natural Science Foundation of Fujian Province of China (2018), Faculty Research Award (2014), and He Yici Chair Professor Award (2018) at Xiamen University, respectively.